Toxic Ultrafine to Nanoparticulate Materials in Wildfire Smoke

Alireza Namayandeh[1,3], Jonathon Howell[1], Sebastian T. Mergelsberg[2], Charlie Lamb[1], Frida Daniela Garcia Ledezma[1], Alex Honeyman[1], Kevin M. Rosso[2], Scott Fendorf[1,3*]

1. Department of Earth System Science, Stanford Doerr School of Sustainability, Stanford University, Stanford, CA, USA.

2. Physical and Computational Sciences Directorate, Pacific Northwest National Laboratory, Richland, USA

3. King Center on Global Development, Stanford University, Stanford, USA

Authors email addresses: arnama@stanford.edu, jh4653@stanford.edu, sebastian.mergelsberg@pnnl.gov, clamb8@stanford.edu, fdgarci2@stanford.edu, honeyman@stanford.edu, Kevin.Rosso@pnnl.gov, fendorf@stanford.edu

Corresponding author:

Scott Fendorf- Current address: Stanford University; 367 Panama St, Stanford, CA 94305, Fendorf@stanford.edu

Preprint statement:

This manuscript is a non-peer-reviewed preprint submitted to EarthArXiv. The manuscript has also been submitted to *Science* for peer review.

Toxic Ultrafine to Nanoparticulate Materials in Wildfire Smoke

Alireza Namayandeh[1,3], Jonathon Howell[1], Sebastian T. Mergelsberg[2], Charlie Lamb[1], Frida Daniela Garcia Ledezma[1], Alex Honeyman[1], Kevin M. Rosso[2], Scott Fendorf[1,3*]

1. Department of Earth System Science, Stanford Doerr School of Sustainability, Stanford University, Stanford, CA, USA.

2. Physical and Computational Sciences Directorate, Pacific Northwest National Laboratory, Richland, USA

3. King Center on Global Development, Stanford University, Stanford, USA

*Corresponding author. Email: Fendorf@stanford.edu

Abstract: Wildfire smoke contains metal-laden ultrafine particles (<0.25 μm) systematically overlooked in air quality monitoring, representing a hidden hazard. We show that these ultrafine particles dominate smoke composition, accounting for >60% of particle mass and carrying toxic metals including chromium, nickel, and titanium at sizes down to 5 nm, small enough to penetrate lung barriers and enter the bloodstream. Unexpectedly, ultrafine metal abundance is decoupled from conventional $PM_{2.5}$ measurements but correlates strongly with underlying geology, revealing that burned lithology controls smoke toxicity. With wildfires intensifying globally and smoke exposure affecting hundreds of millions annually, current exposure assessments based solely on $PM_{2.5}$ mass miss the most hazardous fraction of smoke. Our findings necessitate the incorporation of size-resolved metal composition into air-quality forecasting and public health protection.

Wildfire smoke represents a major source of air pollution and a growing public health problem (*1-6*). Wildfire particulate matter less than 2.5 μm in diameter ($PM_{2.5}$), a pollutant regulated under the Clean Air Act, is more harmful than air pollution from other emission sources, contributing to declining air quality in the United States (*7, 8*), and increasing morbidity (*4, 9-11*) and mortality (*8, 12-15*). Air quality indices use $PM_{2.5}$ concentration as a metric to evaluate air pollution risks in many countries, including the United States, Canada, India, China, and many European countries (*12, 16, 17*). Further, several recent studies (*4, 8, 9, 11-15, 18*) have utilized air modeling and machine learning approaches to measure the health impacts of exposure to wildfire smoke using publicly available $PM_{2.5}$ concentration data. However, $PM_{2.5}$ is an operational and broad term that obscures the chemical and physical diversity of airborne particles, it is a parameter blind to particle chemistry. Current air quality indices offer only a partial assessment of air pollution because they rely solely on bulk $PM_{2.5}$ concentrations, overlooking critical information about variations in particle toxicity.

A wide variety of particles with distinct sizes and morphologies, and thus health impacts, can form within the sub–2.5 μm size range (*19-22*). Ultrafine particles, those < 0.25 μm in diameter, can penetrate deep into lung tissue and tend to be highly reactive with greater tissue contact given their high surface area; they are also not easily cleaned from lung tissue (*23-25*). Included within ultrafine particles are nanoparticles (<0.10 μm), which can move beyond the lung tissue and penetrate the bloodstream and even cross the blood–brain barrier (*23-26*). Recent epidemiological evidence (*23*) demonstrates that exposure to nanoparticles through inhalation is associated with increased risk of neurodegenerative disease, independent of $PM_{2.5}$ mass, suggesting that differences in particle size are likely to influence health outcomes (*23, 24, 27, 28*).

Toxic metals are also disproportionately associated with ultrafine particles, and their health impacts are only beginning to be assessed, but appear severe (*16, 29*). During wildfires, metals can form or associate with ultrafine particles that are often not just fine (<2.5 μm) but predominantly ultrafine (*30, 31*), facilitating their transport through the air and within the human body (*20, 32*). Recent large-scale analyses show that wildfire smoke substantially enriches ambient $PM_{2.5}$ with toxic metals, and that these metal burdens are increasing in frequency and magnitude across fire-impacted regions (*16*). Resolving the chemical and physical aspects (e.g., size, morphology, and co-associations of metal particles) of particles in wildfire smoke, and factors controlling their variation, is thus critical to assess their exposure and health risk (*23, 24, 28, 31, 33, 34*).

Here, we determined the physical and chemical properties of wildfire-derived $PM_{2.5}$ by collecting smoke samples from 10 wildfires across the Western United States during the 2024 fire season. We selected wildfires spanning a wide range of fire characteristics (tables S1 and S2) and smoke $PM_{2.5}$ concentrations (14.0–654 μg m^{-3}) to provide a broad representation of wildfire PM.

Size distribution of smoke

Across the ten wildfires examined, we observe that absolute particle mass in each size fraction in bulk smoke varies significantly but increases on impactor stages with smaller aerodynamic diameters regardless of smoke concentration (Fig. 1A and fig. S1). Averaged across fires, more than 80% of the total mass is associated with stage fractions that are less than 0.50 μm, with over 60% concentrated on stage fractions less than 0.25 μm (Fig. 1B), indicating that ultrafine particles dominate wildfire-smoke mass across all fires. Biomass-burning results in the greatest particle mass within the fine fraction, with volume median diameters typically around 0.25 to 0.30 μm for freshly generated smoke and modest growth with aging (*35-37*). Our measurements alter this picture by showing that wildfire particle mass is not only dominated by fine particles but is strongly shifted toward the ultrafine range (<0.25 μm).

We performed small-angle X-ray scattering (SAXS) on selected filters to further examine the particle size distribution. Excess scattering intensity occurs above background for characteristic sizes of ~2 to 325 nm ($0.002 < q < 0.5$ $Å^{-1}$) (Fig. 2). For most samples, we observe a distinct excess scattering contribution at characteristic sizes of ~2 to 25 nm, indicating an enriched nanoparticle population. The nanoparticle population becomes increasingly pronounced with decreasing aerodynamic diameter, indicating enrichment in the smallest impactor stages (fig. S2). For the 0.50-0.25 μm stage fraction, subtraction of a power law fit to the data results in a continuous excess scattering intensity. For the <0.25 μm stage fraction, equivalent power law fits for PF and BF reveal a distinct population of particles as small as 5 nm, with an average diameter of 61 ± 2 and 66 ± 7 nm, respectively (fig. S3). Wildfire smoke contains substantial ultrafine and nanoparticle mass across sampled fires, which fall well below the size ranges measured in air quality monitoring frameworks, despite dominating the particle population and exerting severe health impacts (*23, 24, 28, 31, 33, 34*).

Toxic metals in smoke

The wildfires we examined also span a wide range of weathering environments with different parent lithologies, from felsic to ultramafic, allowing us to examine source imprints on smoke metal content. Across all wildfires, the total metal concentration varied substantially, ranging from ~200 ng m^{-3} in the Boise Fire (BF) to ~860 ng m^{-3} in the Diamond Complex Fire (DF) (Fig. 3), with metals spanning the full particle size spectrum and a robust and recurring presence in the sub-0.50 μm fraction. Metal concentrations were often highest in the sub-0.25 μm fraction (fig. S4). Individual metal concentrations also varied substantially. For example, Cr ranged from a low of ~37 ng m^{-3} in the Park Fire (PF) to a high of ~604 ng m^{-3} in DF, and Fe ranged from 110 ng m^{-3} in BF to 533 ng m^{-3} in the Middle Fork Complex Fire (MF). Metal concentrations also varied across particle size ranges and consistently extended into the ultrafine (sub-0.25 μm) size fraction. Notably, Cr concentrations are highest in the ultrafine range (<0.25 μm), accounting for ~39% of the ultrafine particles metal mass (ranging from ~20-80% across fires) in comparison to ~20% of the bulk PM metal mass across fires (fig. S5). Iron has the highest average concentration among all measured metals, accounting for ~57% of total metal mass (ranging from ~20-70% across fires) in bulk PM, with ~42% of the ultrafine particle mass (fig. S5). Titanium, Ni, Mn, and Cu together account for ~20% of the total metal in both bulk PM and are distributed across submicron size fractions.

We examined the specific imprint of geology on metal content in smoke by assigning each lithology layer within a wildfire perimeter a relative metal-content score, from felsic (lowest) to ultramafic (highest), and calculated a Geology Composition Index (GCI) by weighting each layer by its area within the fire perimeter (see materials and methods and table S1). We then normalized total metal concentrations by potassium (K), used as a biomass-burning tracer (*38, 39*), to remove variability associated with biomass burning and concentration, and compared these normalized concentrations with the GCI. Metal concentrations increase approximately linearly with increasing GCI ($R^2 = 0.68$), corresponding to a shift from felsic to mafic and ultramafic lithology (Fig. 4A). In addition, the metal fraction in particles with aerodynamic diameter <0.25 μm also shows a strong linear relationship ($R^2 = 0.79$) with increasing GCI (Fig. 4B), indicating that source lithology exerts a strong control over smoke metal composition and size, with fires burning over metal-rich rocks producing greater total toxic metal content and ultrafine metal enrichment (*40, 41*). The geologic imprint is illustrated by the higher metal concentrations observed in Fresno June Lightening Complex Fire (FF), despite having lowest $PM_{2.5}$ concentration, as a result of the fire burning across an area with ~25% mafic and ultramafic rock types; by contrast, the PF with the highest $PM_{2.5}$ concentration burned predominantly over non-mafic, low-metal rocks, resulting in low metal concentrations (fig. S6). We also evaluated whether vegetation type influenced smoke metal levels, but found no discernible relationship.

The individual metal concentrations within $PM_{2.5}$ mass across fires, and total metals across aerodynamic size fractions with $PM_{2.5}$ mass, vary nonlinearly (figs. S7 and S8). We performed the nonparametric Spearman rank correlation test and found that the ratio of metals to $PM_{2.5}$ concentration in the smoke increases with decreasing $PM_{2.5}$ concentration across all size fractions, indicating a consistent negative monotonic relationship (fig. S9), further emphasizing that lower $PM_{2.5}$ concentrations do not equal less toxic PM. Despite the apparent decoupling of total PM and metal content, we find that Cr can serve as a predictor of ultrafine metal PM. Bulk Cr concentration shows a moderately strong correlation ($R^2 = 0.59$) with the concentration of ultrafine metals (<0.25 μm) across all sampled wildfires (Fig. 4C), providing the possibility to assess the threat of ultrafine metals in aggregate through a simple bulk measurement.

Metal-bearing nanoparticles

To gain greater insight on the chemical and physical properties of metal-bearing particles in the ultrafine (to nano-size) range of wildfire smoke, we performed scanning transmission electron microscopy (STEM) with elemental mapping on selected sub-0.50 μm filters with varied metal concentrations. Within the ultrafine fraction, we observed an abundance of aggregates and discrete particles well below 100 nm, extending to sizes <5 nm across different wildfires, particles classified as nanoparticles (*33, 42*). The nanoparticles exhibit diverse morphologies, ranging from spherical to irregular and chain aggregates, features that are controlled by different burning conditions (*35, 36, 43, 44*). Elemental maps reveal that metals such as Fe, Cr, Ni, Mn, and Ti are associated with the nanoparticles (Fig. 5). Individual nanoparticles can host either a single metal or multiple co-localized metals, indicating that wildfire-derived metals are not necessarily segregated by particle type but frequently co-occur within single particles (*24, 45-47*). Co-exposure to airborne metal toxins may lead to a more pronounced toxicity response (*48-50*) than exposure to single-metal or organic-dominated particles. We also observe organic nanoparticles in wildfire smoke as both isolated particles and chain aggregates, ranging from <10 nm to several hundred nanometers in size (fig. S10).

Metals such as Cr, Ni, and Ti reside in the ultrafine to nano-size fractions. Inhalation of these metals can be toxic regardless of particle size (*51-56*), but their toxicity and health impacts can increase substantially at smaller sizes, where higher reactivity and bioavailability can amplify toxicity responses (*23, 24, 28, 45, 46*). In addition, wildfires often burn for extended periods and can degrade air quality for months (fig. S11), resulting in prolonged exposure of local and regional populations to these ultrafine toxins (*57, 58*). Further, we also observe that on average more than 40% of ultrafine metal particulate mass is composed of Fe, including Fe-containing nanoparticles as small as <5 nm, a size range where even relatively benign Fe can become highly reactive and potentially toxic upon inhalation (*20, 59-61*). In the human body, Fe oxide nanoparticles can undergo redox cycling between Fe(II) and Fe(III), promoting the generation of reactive oxygen species (ROS) through Fenton's reaction (*60, 62*). Nanoparticle-driven ROS generation increases as metal particle size decreases because a larger proportion of catalytic surface groups are available for interaction with tissues at the nanoscale, rising from ~10% at 30 nm to nearly 50% at ~3 nm (*63, 64*). Our results demonstrate that wildfire smoke contains abundant metal-bearing nanoparticles across diverse particle sizes, types, and morphologies, highlighting the importance of resolving particle size and composition when assessing exposure to PM in wildfire smoke.

The health and air quality implications of our results point to a common need: to move beyond bulk $PM_{2.5}$ mass toward metrics that better reflect the toxicity of wildfire smoke. Despite their far-reaching impacts on public health, the particle size and chemical composition of PM in wildfire smoke are not effectively captured by current exposure frameworks. The toxicity of smoke is largely based on the mass concentration of $PM_{2.5}$ as an indicator of particulate materials in air (*57, 65-67*). However, $PM_{2.5}$ measurements are blind to differences in size and composition of particles that have important implications for human health (*68, 69*). Incorporating these factors into health assessments and air quality metrics is essential to ensure that public guidance accurately reflects exposure risks.

References and Notes

1. R. W. Gan, B. Ford, W. Lassman, G. Pfister, A. Vaidyanathan, E. Fischer, J. Volckens, J. R. Pierce, S. Magzamen, Comparison of wildfire smoke estimation methods and associations with cardiopulmonary-related hospital admissions. *GeoHealth* **1**, 122-136 (2017).
2. S. DeFlorio-Barker, J. Crooks, J. Reyes, A. G. Rappold, Cardiopulmonary Effects of Fine Particulate Matter Exposure among Older Adults, during Wildfire and Non-Wildfire Periods, in the United States 2008-2010. *Environmental health perspectives* **127**, 037006 (2019).
3. A. Rosenthal, E. Stover, R. J. Haar, Health and social impacts of California wildfires and the deficiencies in current recovery resources: An exploratory qualitative study of systems-level issues. *PLOS ONE* **16**, e0248617 (2021).
4. S. Heft-Neal, A. Driscoll, W. Yang, G. Shaw, M. Burke, Associations between wildfire smoke exposure during pregnancy and risk of preterm birth in California. *Environmental Research* **203**, 111872 (2022).
5. N. Berlin Rubin, G. Wong-Parodi, As California burns: the psychology of wildfire- and wildfire smoke-related migration intentions. *Population and Environment* **44**, 15-45 (2022).
6. J. Korsiak, L. Pinault, T. Christidis, R. T. Burnett, M. Abrahamowicz, S. Weichenthal, Long-term exposure to wildfires and cancer incidence in Canada: a population-based observational cohort study. *The Lancet Planetary Health* **6**, e400-e409 (2022).
7. M. Burke, A. Driscoll, S. Heft-Neal, J. Xue, J. Burney, M. Wara, The changing risk and burden of wildfire in the United States. *Proceedings of the National Academy of Sciences* **118**, e2011048118 (2021).
8. M. Burke, M. L. Childs, B. de la Cuesta, M. Qiu, J. Li, C. F. Gould, S. Heft-Neal, M. Wara, The contribution of wildfire to PM2.5 trends in the USA. *Nature* **622**, 761-766 (2023).
9. S. Heft-Neal, C. F. Gould, M. L. Childs, M. V. Kiang, K. C. Nadeau, M. Duggan, E. Bendavid, M. Burke, Emergency department visits respond nonlinearly to wildfire smoke. *Proceedings of the National Academy of Sciences* **120**, e2302409120 (2023).
10. C. Chen, L. Schwarz, N. Rosenthal, M. E. Marlier, T. Benmarhnia, Exploring spatial heterogeneity in synergistic effects of compound climate hazards: Extreme heat and wildfire smoke on cardiorespiratory hospitalizations in California. *Science Advances* **10**, eadj7264 (2024).
11. Y. S. Jung, M. M. Johnson, M. Burke, S. Heft-Neal, M. L. Bondy, R. S. Chinthrajah, M. R. Cullen, L. Nelson, C. Dresser, K. C. Nadeau, Fine Particulate Matter From 2020 California Wildfires and Mental Health–Related Emergency Department Visits. *JAMA Network Open* **8**, e253326-e253326 (2025).

12. M. Qiu, M. Kelp, S. Heft-Neal, X. Jin, C. F. Gould, D. Q. Tong, M. Burke, Evaluating Chemical Transport and Machine Learning Models for Wildfire Smoke PM2.5: Implications for Assessment of Health Impacts. *Environmental Science & Technology* **58**, 22880-22893 (2024).
13. M. Qiu, J. Li, C. F. Gould, R. Jing, M. Kelp, M. L. Childs, J. Wen, Y. Xie, M. Lin, M. V. Kiang, S. Heft-Neal, N. S. Diffenbaugh, M. Burke, Wildfire smoke exposure and mortality burden in the USA under climate change. *Nature* **647**, 935-943 (2025).
14. C. Y. Park, K. Takahashi, S. Fujimori, T. Jansakoo, C. Burton, H. Huang, S. Kou-Giesbrecht, C. P. O. Reyer, M. Mengel, E. Burke, F. Li, S. Hantson, J. Takakura, D. K. Lee, T. Hasegawa, Attributing human mortality from fire PM2.5 to climate change. *Nature Climate Change* **14**, 1193-1200 (2024).
15. C. F. Gould, S. Heft-Neal, M. Johnson, J. Aguilera, M. Burke, K. Nadeau, Health Effects of Wildfire Smoke Exposure. *Annual Review of Medicine* **75**, 277-292 (2024).
16. E. Krasovich Southworth, M. Qiu, C. F. Gould, A. Kawano, J. Wen, S. Heft-Neal, K. Kilpatrick Voss, A. Lopez, S. Fendorf, J. A. Burney, M. Burke, The Influence of Wildfire Smoke on Ambient PM(2.5) Chemical Species Concentrations in the Contiguous US. *Environ Sci Technol* **59**, 2961-2973 (2025).
17. P. K, P. Kumar, A critical evaluation of air quality index models (1960–2021). *Environmental Monitoring and Assessment* **194**, 324 (2022).
18. Q. Zhang, Y. Wang, Q. Xiao, G. Geng, S. J. Davis, X. Liu, J. Yang, J. Liu, W. Huang, C. He, B. Luo, R. V. Martin, M. Brauer, J. T. Randerson, K. He, Long-range PM2.5 pollution and health impacts from the 2023 Canadian wildfires. *Nature* **645**, 672-678 (2025).
19. Y. Yang, B. Chen, J. Hower, M. Schindler, C. Winkler, J. Brandt, R. Di Giulio, J. Ge, M. Liu, Y. Fu, L. Zhang, Y. Chen, S. Priya, M. F. Hochella, Discovery and ramifications of incidental Magnéli phase generation and release from industrial coal-burning. *Nature Communications* **8**, 194 (2017).
20. Q. Zhang, D. Lu, D. Wang, X. Yang, P. Zuo, H. Yang, Q. Fu, Q. Liu, G. Jiang, Separation and Tracing of Anthropogenic Magnetite Nanoparticles in the Urban Atmosphere. *Environmental Science & Technology* **54**, 9274-9284 (2020).
21. H. Zheng, D. Wu, S. Wang, X. Li, L. N. Jin, B. Zhao, S. Li, Y. Sun, Z. Dong, Q. Wu, X. Chen, Y. Liu, J. Chen, H. Tian, Q. Liu, J. Jiang, H. Kan, K. He, H. He, C. Chen, J. Zhao, S. Weichenthal, J. S. Ji, A. J. Cohen, J. Hao, Q. Li, Control of toxicity of fine particulate matter emissions in China. *Nature* **643**, 404-411 (2025).
22. Y. Thomassen, D. G. Ellingsen, S. Hetland, G. Sand, Chemical speciation and sequential extraction of Mn in workroom aerosols: analytical methodology and results from a field study in Mn alloy plants. *Journal of Environmental Monitoring* **3**, 555-559 (2001).
23. Q. Zhu, Y.-L. Deng, Y. Liu, K. Steenland, Associations between Ultrafine Particles and Incident Dementia in Older Adults. *Environmental Science & Technology* **59**, 5443–5451 (2025).
24. D. K. McDaniel, V. M. Ringel-Scaia, H. A. Morrison, S. Coutermarsh-Ott, M. Council-Troche, J. W. Angle, J. B. Perry, G. Davis, W. Leng, V. Minarchick, Y. Yang, B. Chen, S. W. Reece, D. A. Brown, T. E. Cecere, J. M. Brown, K. M. Gowdy, M. F. Hochella, I. C. Allen, Pulmonary Exposure to Magnéli Phase Titanium Suboxides Results in Significant Macrophage Abnormalities and Decreased Lung Function. *Frontiers in Immunology* **10**, 2714 (2019).
25. R. B. Rice, K. Boaggio, N. E. Olson, K. M. Foley, C. P. Weaver, J. D. Sacks, S. R. McDow, A. L. Holder, S. D. LeDuc, Wildfires Increase Concentrations of Hazardous Air Pollutants in Downwind Communities. *Environmental Science & Technology* **57**, 21235-21248 (2023).
26. S. Morais, M. C. Pereira, K. Slezakova, in *Current Topics in Public Health,* A. J. Rodriguez-Morales, Ed. (IntechOpen, London, 2013).
27. X. Meng, Y. Zhou, S. Shi, S. Wang, M. Zaid, H. Zhang, J. Hu, G. Li, H. Kan, M. Zhou, Mortality and long-term exposure to source-specific PM2·5: evidence from a national cohort study in China. *The Lancet Planetary Health* **10**, 101400 (2026).
28. J. Hu, W. Hu, Z. Xu, C. Peng, J. Cheng, F. Rong, Y. Wang, N. Zhang, M. Guan, J. Wei, Y. Yu, Association between exposure to ambient particulate matter and aggression among adolescents: a national school-based study in China. *BMC Public Health* **26**, 50 (2025).
29. M. M. Johnson, A. Kaushik, O. A. Kline, E. M. Smith, X. Zhou, Y. Pat, L. Buergi, J. Aguilera, S. Alkotob, E. M. Simonin, A. Favaro, M. Couto, O. Bennett, R. S. Chinthrajah, E. Parsons, M. Shamji, M. Burke, M. Bondy, M. Akdis, C. A. Akdis, K. C. Nadeau, Immune impacts of fire smoke exposure. *Nature Medicine* **31**, 3110-3120 (2025).
30. J. Wu, Y. Yang, F. Tou, X. Yan, S. Dai, J. C. Hower, B. K. Saikia, M. Kersten, M. F. Hochella, Combustion conditions and feed coals regulating the Fe- and Ti-containing nanoparticles in various coal fly ash. *Journal of Hazardous Materials* **445**, 130482 (2023).

31. J. Wu, F. Tou, Y. Yang, C. Liu, J. C. Hower, M. Baalousha, G. Wang, M. Liu, M. F. Hochella, Jr., Metal-Containing Nanoparticles in Low-Rank Coal-Derived Fly Ash from China: Characterization and Implications toward Human Lung Toxicity. *Environmental Science & Technology* **55**, 6644-6654 (2021).
32. M. Baalousha, M. Desmau, S. A. Singerling, J. P. Webster, S. J. Matiasek, M. A. Stern, C. N. Alpers, Discovery and potential ramifications of reduced iron-bearing nanoparticles—magnetite, wüstite, and zero-valent iron—in wildland–urban interface fire ashes. *Environmental Science: Nano* **9**, 4136-4149 (2022).
33. M. F. Hochella Jr, D. W. Mogk, J. Ranville, I. C. Allen, G. W. Luther, L. C. Marr, B. P. McGrail, M. Murayama, N. P. Qafoku, K. M. J. S. Rosso, Natural, incidental, and engineered nanomaterials and their impacts on the Earth system. *Science* **363**, eaau8299 (2019).
34. W. Möller, K. Felten, K. Sommerer, G. Scheuch, G. Meyer, P. Meyer, K. Häussinger, W. G. Kreyling, Deposition, Retention, and Translocation of Ultrafine Particles from the Central Airways and Lung Periphery. *American Journal of Respiratory and Critical Care Medicine* **177**, 426-432 (2008).
35. J. S. Reid, R. Koppmann, T. F. Eck, D. P. Eleuterio, A review of biomass burning emissions part II: intensive physical properties of biomass burning particles. *Atmos. Chem. Phys.* **5**, 799-825 (2005).
36. J. S. Reid, P. V. Hobbs, Physical and optical properties of young smoke from individual biomass fires in Brazil. *Journal of Geophysical Research: Atmospheres* **103**, 32013-32030 (1998).
37. T. F. Eck, B. N. Holben, J. S. Reid, N. T. O'Neill, J. S. Schafer, O. Dubovik, A. Smirnov, M. A. Yamasoe, P. Artaxo, High aerosol optical depth biomass burning events: A comparison of optical properties for different source regions. *Geophysical Research Letters* **30**, 2035 (2003).
38. J. E. Pachon, R. J. Weber, X. Zhang, J. A. Mulholland, A. G. Russell, Revising the use of potassium (K) in the source apportionment of PM2.5. *Atmospheric Pollution Research* **4**, 14-21 (2013).
39. T. Joo, M. J. Rogers, C. Soong, T. Hass-Mitchell, S. Heo, M. L. Bell, N. L. Ng, D. R. Gentner, Aged and Obscured Wildfire Smoke Associated with Downwind Health Risks. *Environ Sci Technol Lett* **11**, 1340-1347 (2024).
40. A. M. Lopez, J. L. Pacheco, S. Fendorf, Metal toxin threat in wildland fires determined by geology and fire severity. *Nature Communications* **14**, 8007 (2023).
41. A. Namayandeh, C. Lamb, J. L. Sarabia, M. Shakouri, E. Lopes, J. Lezama Pacheco, A. Honeyman, A. Coker, B. Stewart, S. Tikoo, D. Peak, S. Fendorf, Nonlinear Redox Transformations of Chromium in Soil during Wildfire Heating: The Critical Role of Iron Mineralogy. *Environmental Science & Technology* **59**, 27623-27634 (2025).
42. M. F. Hochella, S. K. Lower, P. A. Maurice, R. L. Penn, N. Sahai, D. L. Sparks, B. S. Twining, Nanominerals, Mineral Nanoparticles, and Earth Systems. *Science* **319**, 1631 (2008).
43. J. V. Martins, P. E. Artaxo Netto, P. V. Hobbs, C. Liousse, H. Cachier, Y. Kaufman, A. Plana-Fattori, in *Biomass Burning and Global Change,* J. S. Levine, Ed. (MIT Press, Cambridge, MA, 1996), pp. 716-732.
44. M. Pósfai, R. Simonics, J. Li, P. V. Hobbs, P. R. Buseck, Individual aerosol particles from biomass burning in southern Africa: 1. Compositions and size distributions of carbonaceous particles. *Journal of Geophysical Research: Atmospheres* **108**, 8484 (2003).
45. S. Jonasson, Å. Gustafsson, B. Koch, A. Bucht, Inhalation exposure of nano-scaled titanium dioxide (TiO2) particles alters the inflammatory responses in asthmatic mice. *Inhalation Toxicology* **25**, 179-191 (2013).
46. V. H. Grassian, T. O'Shaughnessy P, A. Adamcakova-Dodd, J. M. Pettibone, P. S. Thorne, Inhalation exposure study of titanium dioxide nanoparticles with a primary particle size of 2 to 5 nm. *Environmental health perspectives* **115**, 397-402 (2007).
47. A. Elder, R. Gelein, V. Silva, T. Feikert, L. Opanashuk, J. Carter, R. Potter, A. Maynard, Y. Ito, J. Finkelstein, G. Oberdörster, Translocation of inhaled ultrafine manganese oxide particles to the central nervous system. *Environmental health perspectives* **114**, 1172-1178 (2006).
48. Y. Yuan, Y. Wu, X. Ge, D. Nie, M. Wang, H. Zhou, M. Chen, In vitro toxicity evaluation of heavy metals in urban air particulate matter on human lung epithelial cells. *Science of The Total Environment* **678**, 301-308 (2019).
49. S. Sun, N. Zheng, S. Wang, Y. Li, S. Hou, Q. An, C. Chen, X. Li, Y. Ji, P. Li, Inhalation Bioaccessibility and Risk Assessment of Metals in PM2.5 Based on a Multiple-Path Particle Dosimetry Model in the Smelting District of Northeast China. *International Journal of Environmental Research and Public Health* **19**, 8915 (2022).
50. Y. Choi, K. Park, I. Kim, S. D. Kim, Combined toxic effect of airborne heavy metals on human lung cell line A549. *Environ Geochem Health* **40**, 271-282 (2018).
51. D. Y. Shin, S. M. Lee, Y. Jang, J. Lee, C. M. Lee, E.-M. Cho, Y. R. Seo, Adverse Human Health Effects of Chromium by Exposure Route: A Comprehensive Review Based on Toxicogenomic Approach. *International Journal of Molecular Sciences* **24**, 3410 (2023).

52. M. Łożyńska, M. Trojanowska, A. Molik, R. Świetlik, Measurement report: Seasonal trends and chemical speciation of chromium(III/VI) in different fractions of urban particulate matter – a case study of Radom, Poland. *Atmos. Chem. Phys.* **25**, 10499-10510 (2025).
53. G. Genchi, A. Carocci, G. Lauria, M. S. Sinicropi, A. Catalano, Nickel: Human Health and Environmental Toxicology. *Int J Environ Res Public Health* **17**, 679 (2020).
54. T. K. Grimsrud, S. R. Berge, T. Haldorsen, A. Andersen, Exposure to Different Forms of Nickel and Risk of Lung Cancer. *American Journal of Epidemiology* **156**, 1123-1132 (2002).
55. R. L. Prueitt, W. Li, Y. C. Chang, P. Boffetta, J. E. Goodman, Systematic review of the potential respiratory carcinogenicity of metallic nickel in humans. *Crit Rev Toxicol* **50**, 605-639 (2020).
56. A. D. Racovita, Titanium Dioxide: Structure, Impact, and Toxicity. *International Journal of Environmental Research and Public Health* **19**, 5681 (2022).
57. D. A. Jaffe, S. M. O'Neill, N. K. Larkin, A. L. Holder, D. L. Peterson, J. E. Halofsky, A. G. Rappold, Wildfire and prescribed burning impacts on air quality in the United States. *J Air Waste Manag Assoc* **70**, 583-615 (2020).
58. K. M. Gu, T. Lee, J. P. Myong, Wildfire Exposure and Respiratory Health: A Comprehensive Review of Emerging Evidence. *Tuberc Respir Dis (Seoul)* **88**, 643-653 (2025).
59. S. V. Torti, F. M. Torti, Winning the war with iron. *Nature Nanotechnology* **14**, 499-500 (2019).
60. V. Valdiglesias, G. Kiliç, C. Costa, N. Fernández-Bertólez, E. Pásaro, J. P. Teixeira, B. Laffon, Effects of iron oxide nanoparticles: Cytotoxicity, genotoxicity, developmental toxicity, and neurotoxicity. *Environmental and Molecular Mutagenesis* **56**, 125-148 (2015).
61. H. M. Fahmy, E. M. Aly, F. F. Mohamed, N. A. Noor, A. A. Elsayed, Neurotoxicity of green- synthesized magnetic iron oxide nanoparticles in different brain areas of wistar rats. *NeuroToxicology* **77**, 80-93 (2020).
62. N. Li, T. Xia, A. E. Nel, The role of oxidative stress in ambient particulate matter-induced lung diseases and its implications in the toxicity of engineered nanoparticles. *Free Radic Biol Med* **44**, 1689-1699 (2008).
63. L. Hao, L. Chen, Oxidative stress responses in different organs of carp (Cyprinus carpio) with exposure to ZnO nanoparticles. *Ecotoxicology and Environmental Safety* **80**, 103-110 (2012).
64. S. Sonwani, S. Madaan, J. Arora, S. Suryanarayan, D. Rangra, N. Mongia, T. Vats, P. Saxena, Inhalation Exposure to Atmospheric Nanoparticles and Its Associated Impacts on Human Health: A Review. *Frontiers in Sustainable Cities* **3**, 690444 (2021).
65. W. Lassman, B. Ford, R. W. Gan, G. Pfister, S. Magzamen, E. V. Fischer, J. R. Pierce, Spatial and temporal estimates of population exposure to wildfire smoke during the Washington state 2012 wildfire season using blended model, satellite, and in situ data. *GeoHealth* **1**, 106-121 (2017).
66. B. Ainslie, R. So, J. Chen, Operational Evaluation of a Wildfire Air Quality Model from a Forecaster Point of View. *Weather and Forecasting* **37**, 681-698 (2022).
67. K. Abdulrahman, Air quality assessment by daily estimation of ground-level PM2.5 concentrations over Baghdad City using MODIS AOD data. *Air Quality, Atmosphere & Health* **18**, 2047-2059 (2025).
68. I. Stavroulas, G. Grivas, P. Michalopoulos, E. Liakakou, A. Bougiatioti, P. Kalkavouras, K. M. Fameli, N. Hatzianastassiou, N. Mihalopoulos, E. Gerasopoulos, Field Evaluation of Low-Cost PM Sensors (Purple Air PA-II) Under Variable Urban Air Quality Conditions, in Greece. *Atmosphere* **11**, 926 (2020).
69. K. Ardon-Dryer, Y. Dryer, J. N. Williams, N. Moghimi, Measurements of PM2.5 with PurpleAir under atmospheric conditions. *Atmos. Meas. Tech.* **13**, 5441-5458 (2020).
1. R. W. Gan, B. Ford, W. Lassman, G. Pfister, A. Vaidyanathan, E. Fischer, J. Volckens, J. R. Pierce, S. Magzamen, Comparison of wildfire smoke estimation methods and associations with cardiopulmonary-related hospital admissions. *GeoHealth* **1**, 122-136 (2017).
2. S. DeFlorio-Barker, J. Crooks, J. Reyes, A. G. Rappold, Cardiopulmonary Effects of Fine Particulate Matter Exposure among Older Adults, during Wildfire and Non-Wildfire Periods, in the United States 2008-2010. *Environmental health perspectives* **127**, 037006 (2019).
3. A. Rosenthal, E. Stover, R. J. Haar, Health and social impacts of California wildfires and the deficiencies in current recovery resources: An exploratory qualitative study of systems-level issues. *PLOS ONE* **16**, e0248617 (2021).
4. S. Heft-Neal, A. Driscoll, W. Yang, G. Shaw, M. Burke, Associations between wildfire smoke exposure during pregnancy and risk of preterm birth in California. *Environmental Research* **203**, 111872 (2022).
5. N. Berlin Rubin, G. Wong-Parodi, As California burns: the psychology of wildfire- and wildfire smoke-related migration intentions. *Population and Environment* **44**, 15-45 (2022).
6. J. Korsiak, L. Pinault, T. Christidis, R. T. Burnett, M. Abrahamowicz, S. Weichenthal, Long-term exposure to wildfires and cancer incidence in Canada: a population-based observational cohort study. *The Lancet Planetary Health* **6**, e400-e409 (2022).

7. M. Burke, A. Driscoll, S. Heft-Neal, J. Xue, J. Burney, M. Wara, The changing risk and burden of wildfire in the United States. *Proceedings of the National Academy of Sciences* **118**, e2011048118 (2021).
8. M. Burke, M. L. Childs, B. de la Cuesta, M. Qiu, J. Li, C. F. Gould, S. Heft-Neal, M. Wara, The contribution of wildfire to PM2.5 trends in the USA. *Nature* **622**, 761-766 (2023).
9. S. Heft-Neal, C. F. Gould, M. L. Childs, M. V. Kiang, K. C. Nadeau, M. Duggan, E. Bendavid, M. Burke, Emergency department visits respond nonlinearly to wildfire smoke. *Proceedings of the National Academy of Sciences* **120**, e2302409120 (2023).
10. C. Chen, L. Schwarz, N. Rosenthal, M. E. Marlier, T. Benmarhnia, Exploring spatial heterogeneity in synergistic effects of compound climate hazards: Extreme heat and wildfire smoke on cardiorespiratory hospitalizations in California. *Science Advances* **10**, eadj7264 (2024).
11. Y. S. Jung, M. M. Johnson, M. Burke, S. Heft-Neal, M. L. Bondy, R. S. Chinthrajah, M. R. Cullen, L. Nelson, C. Dresser, K. C. Nadeau, Fine Particulate Matter From 2020 California Wildfires and Mental Health–Related Emergency Department Visits. *JAMA Network Open* **8**, e253326-e253326 (2025).
12. M. Qiu, M. Kelp, S. Heft-Neal, X. Jin, C. F. Gould, D. Q. Tong, M. Burke, Evaluating Chemical Transport and Machine Learning Models for Wildfire Smoke PM2.5: Implications for Assessment of Health Impacts. *Environmental Science & Technology* **58**, 22880-22893 (2024).
13. M. Qiu, J. Li, C. F. Gould, R. Jing, M. Kelp, M. L. Childs, J. Wen, Y. Xie, M. Lin, M. V. Kiang, S. Heft-Neal, N. S. Diffenbaugh, M. Burke, Wildfire smoke exposure and mortality burden in the USA under climate change. *Nature* **647**, 935-943 (2025).
14. C. Y. Park, K. Takahashi, S. Fujimori, T. Jansakoo, C. Burton, H. Huang, S. Kou-Giesbrecht, C. P. O. Reyer, M. Mengel, E. Burke, F. Li, S. Hantson, J. Takakura, D. K. Lee, T. Hasegawa, Attributing human mortality from fire PM2.5 to climate change. *Nature Climate Change* **14**, 1193-1200 (2024).
15. C. F. Gould, S. Heft-Neal, M. Johnson, J. Aguilera, M. Burke, K. Nadeau, Health Effects of Wildfire Smoke Exposure. *Annual Review of Medicine* **75**, 277-292 (2024).
16. E. Krasovich Southworth, M. Qiu, C. F. Gould, A. Kawano, J. Wen, S. Heft-Neal, K. Kilpatrick Voss, A. Lopez, S. Fendorf, J. A. Burney, M. Burke, The Influence of Wildfire Smoke on Ambient PM(2.5) Chemical Species Concentrations in the Contiguous US. *Environ Sci Technol* **59**, 2961-2973 (2025).
17. P. K, P. Kumar, A critical evaluation of air quality index models (1960–2021). *Environmental Monitoring and Assessment* **194**, 324 (2022).
18. Q. Zhang, Y. Wang, Q. Xiao, G. Geng, S. J. Davis, X. Liu, J. Yang, J. Liu, W. Huang, C. He, B. Luo, R. V. Martin, M. Brauer, J. T. Randerson, K. He, Long-range PM2.5 pollution and health impacts from the 2023 Canadian wildfires. *Nature* **645**, 672-678 (2025).
19. Y. Yang, B. Chen, J. Hower, M. Schindler, C. Winkler, J. Brandt, R. Di Giulio, J. Ge, M. Liu, Y. Fu, L. Zhang, Y. Chen, S. Priya, M. F. Hochella, Discovery and ramifications of incidental Magnéli phase generation and release from industrial coal-burning. *Nature Communications* **8**, 194 (2017).
20. Q. Zhang, D. Lu, D. Wang, X. Yang, P. Zuo, H. Yang, Q. Fu, Q. Liu, G. Jiang, Separation and Tracing of Anthropogenic Magnetite Nanoparticles in the Urban Atmosphere. *Environmental Science & Technology* **54**, 9274-9284 (2020).
21. H. Zheng, D. Wu, S. Wang, X. Li, L. N. Jin, B. Zhao, S. Li, Y. Sun, Z. Dong, Q. Wu, X. Chen, Y. Liu, J. Chen, H. Tian, Q. Liu, J. Jiang, H. Kan, K. He, H. He, C. Chen, J. Zhao, S. Weichenthal, J. S. Ji, A. J. Cohen, J. Hao, Q. Li, Control of toxicity of fine particulate matter emissions in China. *Nature* **643**, 404-411 (2025).
22. Y. Thomassen, D. G. Ellingsen, S. Hetland, G. Sand, Chemical speciation and sequential extraction of Mn in workroom aerosols: analytical methodology and results from a field study in Mn alloy plants. *Journal of Environmental Monitoring* **3**, 555-559 (2001).
23. Q. Zhu, Y.-L. Deng, Y. Liu, K. Steenland, Associations between Ultrafine Particles and Incident Dementia in Older Adults. *Environmental Science & Technology* **59**, 5443–5451 (2025).
24. D. K. McDaniel, V. M. Ringel-Scaia, H. A. Morrison, S. Coutermarsh-Ott, M. Council-Troche, J. W. Angle, J. B. Perry, G. Davis, W. Leng, V. Minarchick, Y. Yang, B. Chen, S. W. Reece, D. A. Brown, T. E. Cecere, J. M. Brown, K. M. Gowdy, M. F. Hochella, I. C. Allen, Pulmonary Exposure to Magnéli Phase Titanium Suboxides Results in Significant Macrophage Abnormalities and Decreased Lung Function. *Frontiers in Immunology* **10**, 2714 (2019).
25. R. B. Rice, K. Boaggio, N. E. Olson, K. M. Foley, C. P. Weaver, J. D. Sacks, S. R. McDow, A. L. Holder, S. D. LeDuc, Wildfires Increase Concentrations of Hazardous Air Pollutants in Downwind Communities. *Environmental Science & Technology* **57**, 21235-21248 (2023).
26. S. Morais, M. C. Pereira, K. Slezakova, in *Current Topics in Public Health,* A. J. Rodriguez-Morales, Ed. (IntechOpen, London, 2013).

27. X. Meng, Y. Zhou, S. Shi, S. Wang, M. Zaid, H. Zhang, J. Hu, G. Li, H. Kan, M. Zhou, Mortality and long-term exposure to source-specific PM2·5: evidence from a national cohort study in China. *The Lancet Planetary Health* **10**, 101400 (2026).
28. J. Hu, W. Hu, Z. Xu, C. Peng, J. Cheng, F. Rong, Y. Wang, N. Zhang, M. Guan, J. Wei, Y. Yu, Association between exposure to ambient particulate matter and aggression among adolescents: a national school-based study in China. *BMC Public Health* **26**, 50 (2025).
29. M. M. Johnson, A. Kaushik, O. A. Kline, E. M. Smith, X. Zhou, Y. Pat, L. Buergi, J. Aguilera, S. Alkotob, E. M. Simonin, A. Favaro, M. Couto, O. Bennett, R. S. Chinthrajah, E. Parsons, M. Shamji, M. Burke, M. Bondy, M. Akdis, C. A. Akdis, K. C. Nadeau, Immune impacts of fire smoke exposure. *Nature Medicine* **31**, 3110-3120 (2025).
30. J. Wu, Y. Yang, F. Tou, X. Yan, S. Dai, J. C. Hower, B. K. Saikia, M. Kersten, M. F. Hochella, Combustion conditions and feed coals regulating the Fe- and Ti-containing nanoparticles in various coal fly ash. *Journal of Hazardous Materials* **445**, 130482 (2023).
31. J. Wu, F. Tou, Y. Yang, C. Liu, J. C. Hower, M. Baalousha, G. Wang, M. Liu, M. F. Hochella, Jr., Metal-Containing Nanoparticles in Low-Rank Coal-Derived Fly Ash from China: Characterization and Implications toward Human Lung Toxicity. *Environmental Science & Technology* **55**, 6644-6654 (2021).
32. M. Baalousha, M. Desmau, S. A. Singerling, J. P. Webster, S. J. Matiasek, M. A. Stern, C. N. Alpers, Discovery and potential ramifications of reduced iron-bearing nanoparticles—magnetite, wüstite, and zero-valent iron—in wildland–urban interface fire ashes. *Environmental Science: Nano* **9**, 4136-4149 (2022).
33. M. F. Hochella Jr, D. W. Mogk, J. Ranville, I. C. Allen, G. W. Luther, L. C. Marr, B. P. McGrail, M. Murayama, N. P. Qafoku, K. M. J. S. Rosso, Natural, incidental, and engineered nanomaterials and their impacts on the Earth system. *Science* **363**, eaau8299 (2019).
34. W. Möller, K. Felten, K. Sommerer, G. Scheuch, G. Meyer, P. Meyer, K. Häussinger, W. G. Kreyling, Deposition, Retention, and Translocation of Ultrafine Particles from the Central Airways and Lung Periphery. *American Journal of Respiratory and Critical Care Medicine* **177**, 426-432 (2008).
35. J. S. Reid, R. Koppmann, T. F. Eck, D. P. Eleuterio, A review of biomass burning emissions part II: intensive physical properties of biomass burning particles. *Atmos. Chem. Phys.* **5**, 799-825 (2005).
36. J. S. Reid, P. V. Hobbs, Physical and optical properties of young smoke from individual biomass fires in Brazil. *Journal of Geophysical Research: Atmospheres* **103**, 32013-32030 (1998).
37. T. F. Eck, B. N. Holben, J. S. Reid, N. T. O'Neill, J. S. Schafer, O. Dubovik, A. Smirnov, M. A. Yamasoe, P. Artaxo, High aerosol optical depth biomass burning events: A comparison of optical properties for different source regions. *Geophysical Research Letters* **30**, 2035 (2003).
38. J. E. Pachon, R. J. Weber, X. Zhang, J. A. Mulholland, A. G. Russell, Revising the use of potassium (K) in the source apportionment of PM2.5. *Atmospheric Pollution Research* **4**, 14-21 (2013).
39. T. Joo, M. J. Rogers, C. Soong, T. Hass-Mitchell, S. Heo, M. L. Bell, N. L. Ng, D. R. Gentner, Aged and Obscured Wildfire Smoke Associated with Downwind Health Risks. *Environ Sci Technol Lett* **11**, 1340-1347 (2024).
40. A. M. Lopez, J. L. Pacheco, S. Fendorf, Metal toxin threat in wildland fires determined by geology and fire severity. *Nature Communications* **14**, 8007 (2023).
41. A. Namayandeh, C. Lamb, J. L. Sarabia, M. Shakouri, E. Lopes, J. Lezama Pacheco, A. Honeyman, A. Coker, B. Stewart, S. Tikoo, D. Peak, S. Fendorf, Nonlinear Redox Transformations of Chromium in Soil during Wildfire Heating: The Critical Role of Iron Mineralogy. *Environmental Science & Technology* **59**, 27623-27634 (2025).
42. M. F. Hochella, S. K. Lower, P. A. Maurice, R. L. Penn, N. Sahai, D. L. Sparks, B. S. Twining, Nanominerals, Mineral Nanoparticles, and Earth Systems. *Science* **319**, 1631 (2008).
43. J. V. Martins, P. E. Artaxo Netto, P. V. Hobbs, C. Liousse, H. Cachier, Y. Kaufman, A. Plana-Fattori, in *Biomass Burning and Global Change,* J. S. Levine, Ed. (MIT Press, Cambridge, MA, 1996), pp. 716-732.
44. M. Pósfai, R. Simonics, J. Li, P. V. Hobbs, P. R. Buseck, Individual aerosol particles from biomass burning in southern Africa: 1. Compositions and size distributions of carbonaceous particles. *Journal of Geophysical Research: Atmospheres* **108**, 8484 (2003).
45. S. Jonasson, Å. Gustafsson, B. Koch, A. Bucht, Inhalation exposure of nano-scaled titanium dioxide (TiO2) particles alters the inflammatory responses in asthmatic mice. *Inhalation Toxicology* **25**, 179-191 (2013).
46. V. H. Grassian, T. O'Shaughnessy P, A. Adamcakova-Dodd, J. M. Pettibone, P. S. Thorne, Inhalation exposure study of titanium dioxide nanoparticles with a primary particle size of 2 to 5 nm. *Environmental health perspectives* **115**, 397-402 (2007).
47. A. Elder, R. Gelein, V. Silva, T. Feikert, L. Opanashuk, J. Carter, R. Potter, A. Maynard, Y. Ito, J. Finkelstein, G. Oberdörster, Translocation of inhaled ultrafine manganese oxide particles to the central nervous system. *Environmental health perspectives* **114**, 1172-1178 (2006).

48. Y. Yuan, Y. Wu, X. Ge, D. Nie, M. Wang, H. Zhou, M. Chen, In vitro toxicity evaluation of heavy metals in urban air particulate matter on human lung epithelial cells. *Science of The Total Environment* **678**, 301-308 (2019).
49. S. Sun, N. Zheng, S. Wang, Y. Li, S. Hou, Q. An, C. Chen, X. Li, Y. Ji, P. Li, Inhalation Bioaccessibility and Risk Assessment of Metals in PM2.5 Based on a Multiple-Path Particle Dosimetry Model in the Smelting District of Northeast China. *International Journal of Environmental Research and Public Health* **19**, 8915 (2022).
50. Y. Choi, K. Park, I. Kim, S. D. Kim, Combined toxic effect of airborne heavy metals on human lung cell line A549. *Environ Geochem Health* **40**, 271-282 (2018).
51. D. Y. Shin, S. M. Lee, Y. Jang, J. Lee, C. M. Lee, E.-M. Cho, Y. R. Seo, Adverse Human Health Effects of Chromium by Exposure Route: A Comprehensive Review Based on Toxicogenomic Approach. *International Journal of Molecular Sciences* **24**, 3410 (2023).
52. M. Łożyńska, M. Trojanowska, A. Molik, R. Świetlik, Measurement report: Seasonal trends and chemical speciation of chromium(III/VI) in different fractions of urban particulate matter – a case study of Radom, Poland. *Atmos. Chem. Phys.* **25**, 10499-10510 (2025).
53. G. Genchi, A. Carocci, G. Lauria, M. S. Sinicropi, A. Catalano, Nickel: Human Health and Environmental Toxicology. *Int J Environ Res Public Health* **17**, 679 (2020).
54. T. K. Grimsrud, S. R. Berge, T. Haldorsen, A. Andersen, Exposure to Different Forms of Nickel and Risk of Lung Cancer. *American Journal of Epidemiology* **156**, 1123-1132 (2002).
55. R. L. Prueitt, W. Li, Y. C. Chang, P. Boffetta, J. E. Goodman, Systematic review of the potential respiratory carcinogenicity of metallic nickel in humans. *Crit Rev Toxicol* **50**, 605-639 (2020).
56. A. D. Racovita, Titanium Dioxide: Structure, Impact, and Toxicity. *International Journal of Environmental Research and Public Health* **19**, 5681 (2022).
57. D. A. Jaffe, S. M. O'Neill, N. K. Larkin, A. L. Holder, D. L. Peterson, J. E. Halofsky, A. G. Rappold, Wildfire and prescribed burning impacts on air quality in the United States. *J Air Waste Manag Assoc* **70**, 583-615 (2020).
58. K. M. Gu, T. Lee, J. P. Myong, Wildfire Exposure and Respiratory Health: A Comprehensive Review of Emerging Evidence. *Tuberc Respir Dis (Seoul)* **88**, 643-653 (2025).
59. S. V. Torti, F. M. Torti, Winning the war with iron. *Nature Nanotechnology* **14**, 499-500 (2019).
60. V. Valdiglesias, G. Kiliç, C. Costa, N. Fernández-Bertólez, E. Pásaro, J. P. Teixeira, B. Laffon, Effects of iron oxide nanoparticles: Cytotoxicity, genotoxicity, developmental toxicity, and neurotoxicity. *Environmental and Molecular Mutagenesis* **56**, 125-148 (2015).
61. H. M. Fahmy, E. M. Aly, F. F. Mohamed, N. A. Noor, A. A. Elsayed, Neurotoxicity of green- synthesized magnetic iron oxide nanoparticles in different brain areas of wistar rats. *NeuroToxicology* **77**, 80-93 (2020).
62. N. Li, T. Xia, A. E. Nel, The role of oxidative stress in ambient particulate matter-induced lung diseases and its implications in the toxicity of engineered nanoparticles. *Free Radic Biol Med* **44**, 1689-1699 (2008).
63. L. Hao, L. Chen, Oxidative stress responses in different organs of carp (Cyprinus carpio) with exposure to ZnO nanoparticles. *Ecotoxicology and Environmental Safety* **80**, 103-110 (2012).
64. S. Sonwani, S. Madaan, J. Arora, S. Suryanarayan, D. Rangra, N. Mongia, T. Vats, P. Saxena, Inhalation Exposure to Atmospheric Nanoparticles and Its Associated Impacts on Human Health: A Review. *Frontiers in Sustainable Cities* **3**, 690444 (2021).
65. W. Lassman, B. Ford, R. W. Gan, G. Pfister, S. Magzamen, E. V. Fischer, J. R. Pierce, Spatial and temporal estimates of population exposure to wildfire smoke during the Washington state 2012 wildfire season using blended model, satellite, and in situ data. *GeoHealth* **1**, 106-121 (2017).
66. B. Ainslie, R. So, J. Chen, Operational Evaluation of a Wildfire Air Quality Model from a Forecaster Point of View. *Weather and Forecasting* **37**, 681-698 (2022).
67. K. Abdulrahman, Air quality assessment by daily estimation of ground-level PM2.5 concentrations over Baghdad City using MODIS AOD data. *Air Quality, Atmosphere & Health* **18**, 2047-2059 (2025).
68. I. Stavroulas, G. Grivas, P. Michalopoulos, E. Liakakou, A. Bougiatioti, P. Kalkavouras, K. M. Fameli, N. Hatzianastassiou, N. Mihalopoulos, E. Gerasopoulos, Field Evaluation of Low-Cost PM Sensors (Purple Air PA-II) Under Variable Urban Air Quality Conditions, in Greece. *Atmosphere* **11**, 926 (2020).
69. K. Ardon-Dryer, Y. Dryer, J. N. Williams, N. Moghimi, Measurements of PM2.5 with PurpleAir under atmospheric conditions. *Atmos. Meas. Tech.* **13**, 5441-5458 (2020).
70. C. Sioutas, *Development of new generation personal monitors for fine particulate matter (PM) and its metal content*. (Mickey Leland National Urban Air Toxics Research Center, 2004).
71. W. C. Malm, J. F. Sisler, D. Huffman, R. A. Eldred, T. A. Cahill, Spatial and seasonal trends in particle concentration and optical extinction in the United States. *Journal of Geophysical Research: Atmospheres* **99**, 1347-1370 (1994).

72. K. Hans Wedepohl, The composition of the continental crust. *Geochimica et Cosmochimica Acta* **59**, 1217-1232 (1995).
73. S. R. Taylor, S. McLennan, *Planetary Crusts: Their Composition, Origin and Evolution*. (Cambridge University Press, 2009).
74. *Treatise on Geochemistry*. K. K. Turekian, H. D. Holland, Eds., (Elsevier Science, Amsterdam, Netherlands, ed. 2, 2013).
75. S. R. Nockolds, Average Chemical Compositions of Some Igneous Rocks. *GSA Bulletin* **65**, 1007-1032 (1954).

Acknowledgments:

We are grateful to Andrew Barnum from the Stanford Nano Shared Facilities (SNSF) for his support with STEM analysis and Karrie Weaver from Stanford SIGMA Shared Facility for her support with acid digestion and ICP analysis. We also thank Diana Moanga (Stanford Doerr School of Sustainability Spatial Analysis Center) for supporting the geospatial analysis.

Funding: Namayandeh was funded by the National Science Foundation Earth Sciences Postdoctoral Fellowships under grant no. 2403686. The STEM analysis was performed at the Stanford Nano Shared Facilities (SNSF) RRID: SCR_023230, supported by the National Science Foundation under award ECCS-2026822. Mergelsberg and Rosso were supported by the U.S. Department of Energy (DOE), Office of Science, Office of Basic Energy Sciences, Chemical Sciences, Geosciences, and Biosciences Division, through the Geosciences Program (FWP 56674) at Pacific Northwest National Laboratory (PNNL). PNNL is a multiprogram national laboratory operated for the U.S. Department of Energy by Battelle Memorial Institute under Contract No.~DE-AC05-76RL01830. The authors acknowledge the use of facilities and the scientific and technical assistance provided by the Stanford Doerr School of Sustainability's Environmental Measurements Core Facility (RRID: SCR_023255). In addition, part of this work was performed in the SIGMA Shared Facility, with support from the Stanford Doerr School of Sustainability. RRID: SCR_023259.

Author contributions:
Conceptualization: A.N. and S.F.
Sample collection: A.N., J.H., A.H.
Methodology: A.N., J.H., S.M., C.L., F.G.L., K.R., and S.F.
Software: A.N. and C.L.
Formal analysis: A.N., J.H., S.M., C.L.
Data Curation: A.N., J.H., S.M., C.L., F.G.L.
Writing – Original Draft: A.N.
Writing – Review & Editing: A.N., J.H., S.M., C.L., F.G.L., K.R., and S.F.

Competing interests: The authors declare that they have no competing interests.

Data and code Availability: All data are available in the manuscript or the supplementary materials. All data and code to reproduce analyses will be deposited at a permanent URL at the time of publication and are available upon request.

List of Supplementary Materials:

Materials and Methods
Figs. S1 to S16
Tables S1 to S2
References (70-75)
Data S1

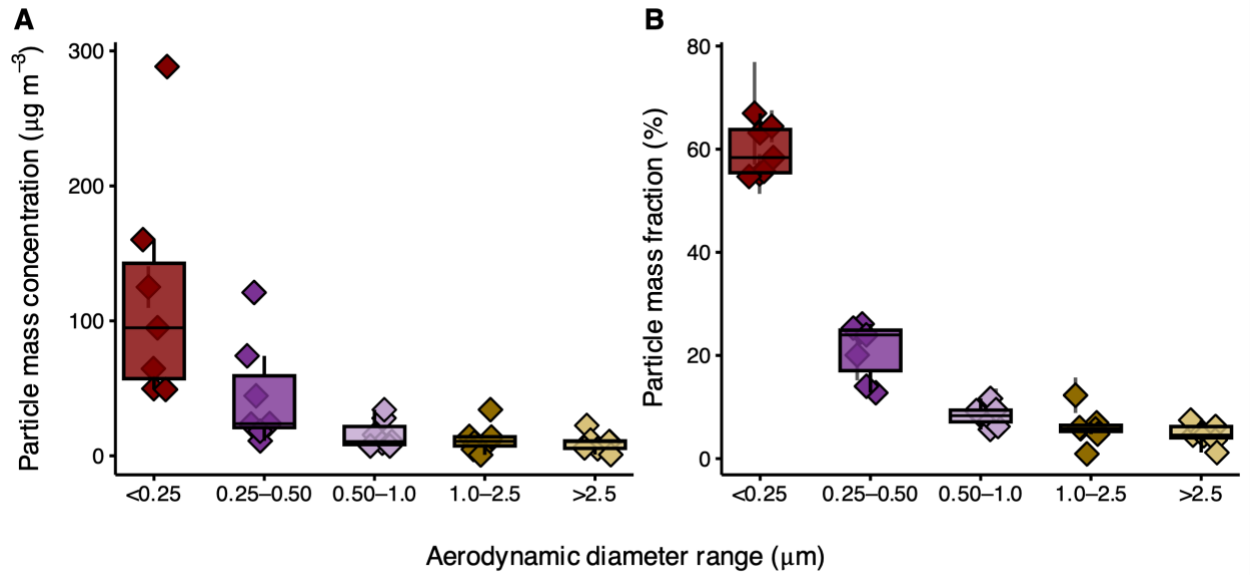

Fig. 1. Distribution of smoke PM mass across aerodynamic diameter ranges. (A) absolute mass of particles, (B) normalized mass of particles, calculated by dividing the mass in each size bin by the total mass. Wildfires include the Park Fire, Boise Fire, Shelly Fire, Dimond Complex Fire, Red Fire, Middle Fork Complex Fire, and Wapiti Fire. The masses from the remaining fires were below the detection limit of the balance.

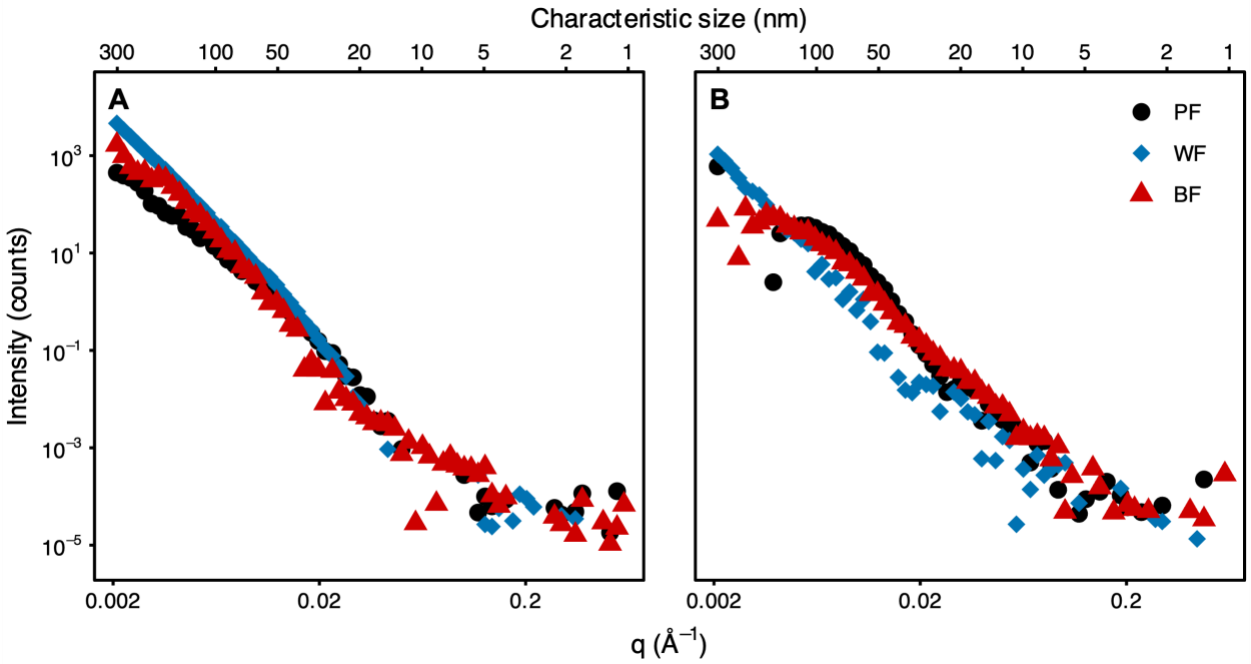

Fig. 2. Power law-subtracted SAXS profiles. (A) 0.5–0.25 µm impactor stage and (B) <0.25 µm impactor stage for the Park Fire (PF), Wapiti Fire (WF), and Boise Fire (BF). These samples were selected because the high particle mass on the filters enabled reliable SAXS measurements. The upper x-axis indicates the corresponding characteristic particle size range probed by the measurements.

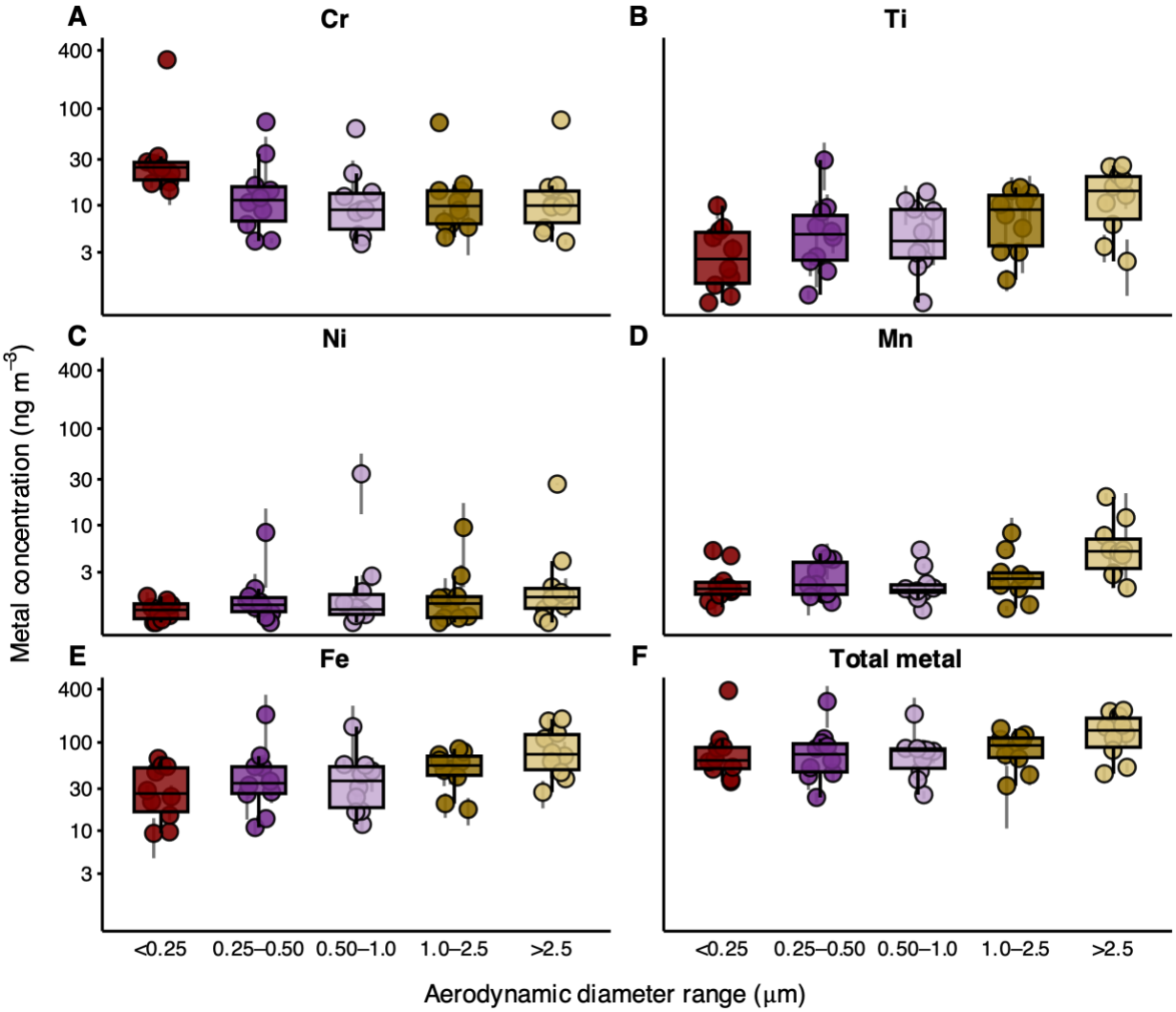

Fig. 3. Distribution of smoke metal concentration across aerodynamic diameter ranges (n=10). Total metal includes Cr, Ti, Ni, Mn, Fe, and Cu. Other metals were excluded due to their low concentrations.

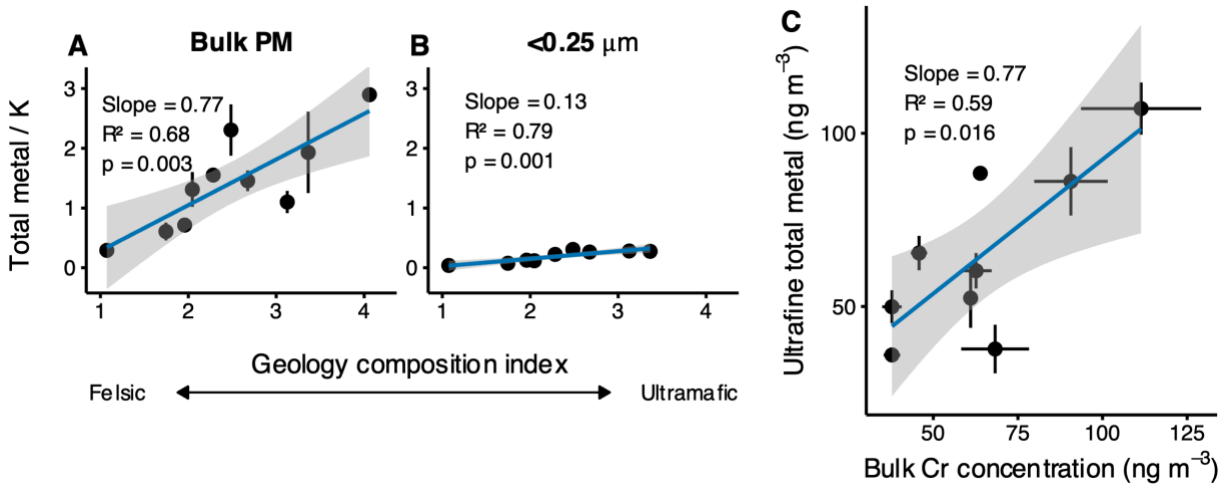

Fig. 4. Geological control on metal abundance in wildfire smoke. (A) Relationship between the lithology composition index (GCI) and the ratio of total metals to bulk K in bulk PM. Metal abundance increases systematically from felsic to ultramafic geological compositions. (B) The same relationship for PM <0.25 µm. Ultrafine particles show a positive relationship with GCI, indicating that geological sources influence metal enrichment even in the smallest smoke particles. GCI reflects the relative contribution of felsic to ultramafic lithologies within each wildfire perimeter. (C) Bulk Cr as a predictor of ultrafine metal enrichment in wildfire smoke. Relationship between bulk Cr concentration and ultrafine total metal mass (<0.25 µm), showing a positive association. Error bars represent standard errors. We evaluated point influence using Cook's distance. For plot A, no observation exceeded the conventional threshold, including the Dimond Complex fire point at the far right (Cook's D = 0.27; 4/n = 0.40), so all fires were retained. For plots B and C, the Dimond Complex exceeded the Cook's distance threshold (D = 3.3 and 18, respectively) and was excluded from the regression. Notably, the excluded sample shows the highest concentrations of GCI, ultrafine total metal, and Cr.

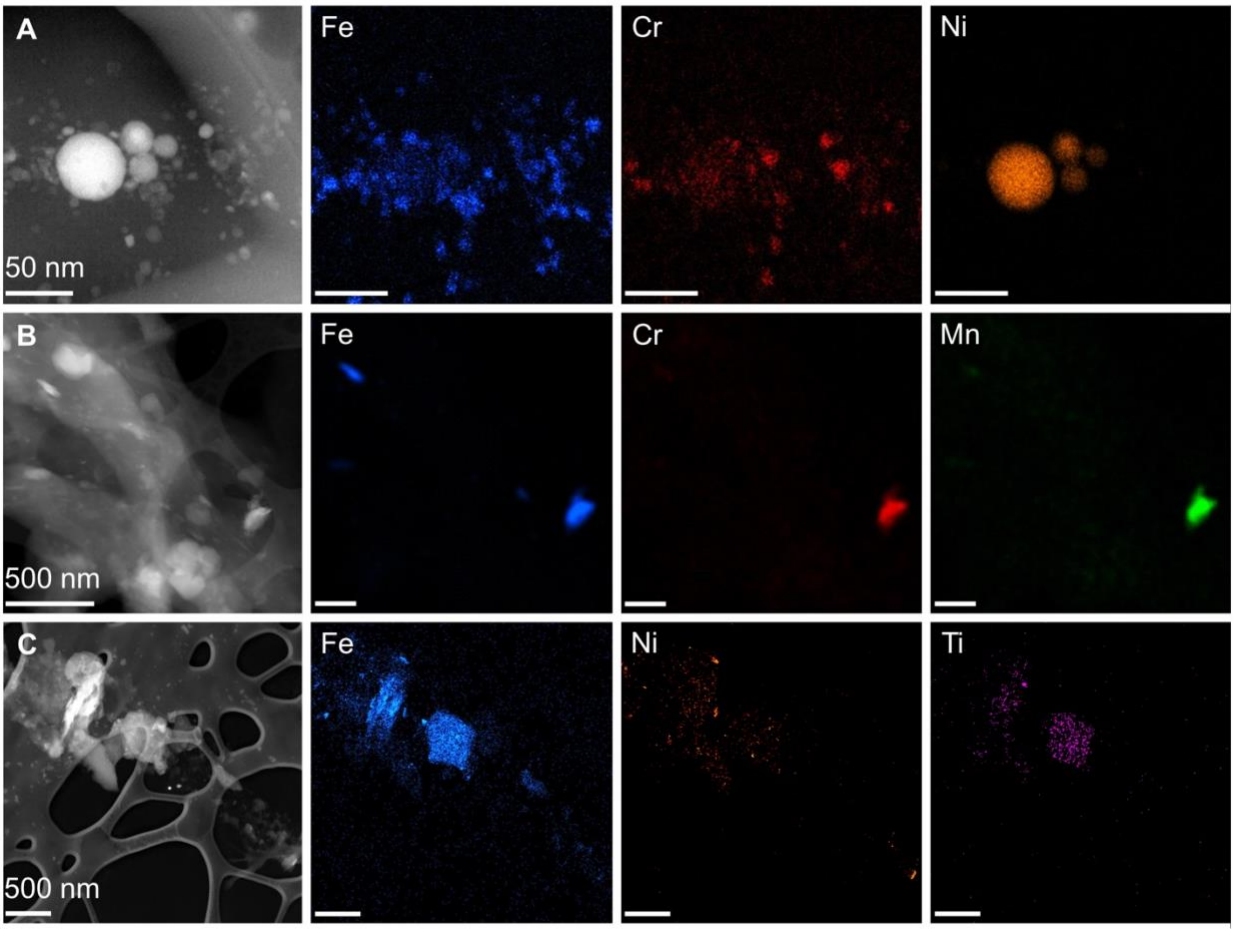

Fig. 5. Scanning transmission electron microscopy (STEM) images and corresponding elemental maps. (A) The Middle Fork Fire, showing Fe, Cr, and Ni nanoparticles with sizes as small as <5 nm. (B) Park Fire, where Fe, Cr, and Mn nanoparticles are co-located within a single particle. (C) Wapiti Fire, showing co-associated Fe, Ni, and Ti nanoparticles forming larger metal-rich particles.

Supplementary Materials for

Toxic Ultrafine to Nanoparticulate Materials in Wildfire Smoke

Alireza Namayandeh[1,3], Jonathon Howell[1], Sebastian T. Mergelsberg[2], Charlie Lamb[1], Frida Daniela Garcia Ledezma[1], Alex Honeyman[1], Kevin M. Rosso[2], Scott Fendorf[1,3*]

1. Department of Earth System Science, Stanford Doerr School of Sustainability, Stanford University, Stanford, CA, USA

2. Physical and Computational Sciences Directorate, Pacific Northwest National Laboratory, Richland, USA

3. King Center on Global Development, Stanford University, Stanford, USA

*Corresponding author. Email: Fendorf@stanford.edu

Supplementary Materials

Materials and Methods
Figs. S1 to S16
Tables S1 to S2
References (70-75)
Data S1

Materials and Methods

Wildfire Smoke Collection

Wildfire smoke was collected from 10 active wildfires across the western United States between June and September 2024, which we term the 2024 wildfire season. Included in our sampling are the Fresno June Lightning Complex Fire (FF), Lake Fire (LF), Coffee Pot Fire (CF), Park Fire (PF), Boise Fire (BF), and Shelly Fire (SF), from California (CA), Dimond Complex Fire (DF) and Red Fire (RF) from Oregon (OR), and Middle Fork Complex Fire (MF) and Wapiti Fire (WF) from Idaho (ID). The wildfire locations, sampling dates, dominant vegetation, and the distance of the sampling location from the wildfire are shown in table S2.

The wildfires occurred on diverse geological settings from felsic to ultramafic and a range of smoke $PM_{2.5}$ concentrations to capture the full spectrum of Air Quality Index (AQI) $PM_{2.5}$ categories, from moderate to hazardous. AQI was used as a reference because communities affected by these wildfires were receiving public health guidance based on AQI levels. PurpleAir real-time air quality monitoring sensors were used to guide site selection, ensuring that sampling occurred within the smoke plume and in locations where smoke $PM_{2.5}$ concentrations were at least within the moderate range (9.1-35.4 μg m^{-3}) in the vicinity of the wildfires (fig. S11). Additionally, we utilized an EPAM-5000 Environmental Particulate Air Monitor Kit (SKC) equipped with a 2.5-μm impactor to measure real-time $PM_{2.5}$ concentrations during sampling (fig. S12). The smoke plume data were downloaded from NOAA's Hazard Mapping System (HMS) and visualized for the day of sampling for each sample location to further confirm the presence of the smoke during sample collection (fig. S13). The fire perimeters were downloaded from National Interagency Fire Center. We used ArcGIS Pro to overlay different layers of information for the plum maps.

Smoke samples were collected using a Flite 4 Area Sample Pump (SKC) connected to a Sioutas Cascade Impactor (SKC), which separated and collected airborne PM on polytetrafluoroethylene (PTFE) filters into five size fractions (50% cut-points): >2.5, 1.0–2.5, 0.50–1.0, 0.25–0.50, and <0.25 μm. The efficiency of the Sioutas Cascade Impactors in separating airborne PM across these cut-points was previously evaluated, showing a collection efficiency above 90%.(*70*) A picture of particles collected on the filters for selected wildfires is shown in fig. S14.

Smoke Particle Size Distribution

Before and after sample collection, the filters were weighed using a microbalance (Mettler Toledo XPR2) to determine the mass of particles on each filter, and thus, their size distribution. Additionally, small-angle X-ray scattering (SAXS) was performed on selected smoke samples (PF, WF, and BF) to confirm the presence of nanoparticles and quantify their dominant size distributions. These samples were selected due to their high particle mass loadings, which provided sufficient material for SAXS measurements. Data were collected using a laboratory-based Xenocs Xeuss 3.0 instrument (Grenoble, France) equipped with a monochromatic Cu Kα X-ray source (λ = 1.541891 Å). Measurements were acquired at sample-to-detector distances (s2d) of 50 and 370 mm using a Dectris Eiger2 R 1M detector (Baden-Daettwil, Switzerland). LaB_6 and silver behenate standards (Sigma-Aldrich, Burlington, MA, USA) were used to calibrate the sample-to-detector distance and refine detector alignment relative to the incident X-ray beam. Filter samples were cut into approximately 5 × 5 mm sections and mounted onto indexed sample holders using tape. Due to the impactor disk configuration, particles were deposited along a narrow line at the center of filters >2.5, 2.5–1.0, 1.0–0.50, and 0.50–0.25 μm, whereas particles were more evenly distributed across the filter <0.25 (fig. S14). For filters >2.5, 2.5–1.0, 1.0–0.50, and 0.50–0.25 μm samples were raster-scanned at 0.1 mm intervals with 0.1 s exposure times to identify regions with the highest particle loading, which were subsequently selected for SAXS measurements. Background scattering was collected by translating the beam 1 mm to either side of the sample region to measure scattering from the filter substrate alone. In all cases, background scattering was constant, and only sample positions exhibited scattering profiles consistent with a particle size distribution. For filter <0.25 μm, SAXS measurements were performed directly on the sample regions, and background scattering was collected from two unused filters. Each sample position was measured with an exposure time of 30 minutes per image. Data reduction and analysis were performed using Irena (Ilavsky and Jemian, 2009) within Igor Pro 9 (WaveMetrics, Lake Oswego, OR, USA). To examine the particle scattering independent of the scattering from larger aggregates, a power law was subtracted from the data of the form I(q) = A*q^-P+C, where A is a scalar, P is an exponent, and C is the background. A and P were fit at low q (0.002 to 0.003), and C was fit to high q (0.3 to 0.5). At values of P close to 4, this function approximates the scattering of random aggregates much larger than the size range of interest. Values of P close to 2 for the < 0.25 μm stages indicate a significant scattering background due to correlations between the filter material and the powder.

Wildfire Smoke Composition

The smoke samples collected on PTFE filters were totally digested in a microwave digester using a mixture of nitric acid (HNO_3, 67–70%), hydrochloric acid (HCl, 36–38%), and hydrofluoric acid (HF, 49%). All acids used were Optima-grade reagents. The elemental composition of the digested samples was then analyzed using a Neptune XT multicollector inductively coupled plasma mass spectrometer (MC-ICP-MS). In addition, the chemical composition of ambient $PM_{2.5}$ at each sampling location, spanning the period from before the wildfire start date through after our sampling date, was obtained from the Federal Land Manager Environmental Database (FED), maintained by the National Park Service and the U.S. Forest Service (*71*). We extracted daily, monitor-level chemical concentration data from the Environmental Protection Agency's $PM_{2.5}$ Chemical Speciation Network (CSN) and the Interagency Monitoring of Protected Visual Environments (IMPROVE) program. Examining metal concentrations reported by national air monitoring networks, for the 10 wildfires, metal levels remain persistent for days, with little fluctuation before and after our sample collection day (Figs. S15 and S16). The locations and distances of each sensor to the wildfire and our sampling location are shown in fig. S13 and table S2.

Geology Composition Index Model

To evaluate the influence of geology on wildfire smoke metal concentrations, we developed a Geology Composition Index (GCI) for each fire based on the lithologic composition within the fire perimeter. Lithological units intersecting each wildfire perimeter were obtained from the Cooperative National Geologic Map, and the fire perimeters were downloaded from the National Interagency Fire Center. The corresponding acreage of each lithological unit within the fire perimeter was calculated in ArcGIS (table S1). The geological maps for each sample location are shown in fig. S6.

Each lithological unit was assigned a relative metal-content score reflecting the typical abundance of transition metals in major rock types. Scores were assigned according to the general geochemical enrichment of mafic and ultramafic lithologies relative to felsic rocks. Felsic lithologies (e.g., granite, rhyolite) were assigned the lowest score (1). Felsic-to-intermediate compositions (e.g., granodiorite and dacite) were assigned a score of 2.5. Intermediate lithologies (e.g., andesite, diorite) were assigned a score of 4. Intermediate-to-mafic lithologies were assigned a score of 4.5, mafic lithologies (e.g., basalt, gabbro) were assigned higher scores (5), and ultramafic lithologies (e.g., serpentinite) were assigned the highest score (5.5). Geological units dominated by sedimentary or metasedimentary materials with low metal content, such as sandstone, were assigned a lower baseline score (1), reflecting their typically lower concentrations of transition metals relative to mafic and ultramafic lithologies. Metamorphic rocks were scored according to their protolith. For example, rocks derived from low-metal compositions were assigned a score of 1, whereas rocks derived from mafic compositions were assigned a score of 5. These assignments follow well-established global geochemical trends in which Fe, Cr, Ni, Ti, Mn, and other transition metals increase systematically from felsic to ultramafic rocks (*72-75*). Because total metal concentrations in wildfire smoke are strongly influenced by Fe, we ensured that these scores reflect the relative average concentration of Fe across different rock types (*75*).

To ensure consistent classification across all fires, geological descriptions for each mapped unit were evaluated using a rule-based text classification approach. Lithologic descriptions were parsed to identify diagnostic mineralogical and compositional terms (e.g., granite, rhyolite, granodiorite, andesite, basalt, serpentinite, peridotite) and to identify compositional ranges or mixed lithologies. Where geological descriptions contained multiple lithologies, dominance terms (e.g., "mostly", "primarily", "dominantly") were used to weight the classification toward the dominant rock type.

The GCI for each wildfire was calculated as the acreage-weighted mean of the lithologic scores within the fire perimeter:

$$GCI = \sum_i f_i \times S_i$$

where S_i is the assigned lithologic score for geological layer i, and fi is the fractional area of that layer within the fire perimeter. This approach produces a single fire-level index that represents the overall metal-enrichment potential of the geological materials exposed within the burned area for each wildfire.

Morphology, size, and distribution of metal-bearing particles

Scanning transmission electron microscopy (STEM) was used to examine the size, morphology, and elemental distribution of smoke particles. Selected filters were cut and sonicated in ultrapure water (18.2 MΩ) for 3-5 minutes. The temperature was maintained below 25 °C by adding crushed ice throughout the sonication process. A droplet of the resulting suspension was then deposited onto a lacy carbon TEM grid (Ted Pella) using a micropipette and allowed to air dry for 12 hours. An additional droplet was deposited onto a silicon nitride TEM grid (Ted Pella) to map the organic particulates. STEM images were acquired using a high-angle annular dark-field (HAADF) detector. Elemental maps were subsequently obtained with a Thermo Fisher Spectra 300 monochromated, double-corrected STEM equipped with SuperX energy-dispersive X-ray spectroscopy (EDS) detectors. The brightness and contrast of the images were linearly adjusted across each image to minimize the signal-to-noise ratio of the mapped pixels.

870 **Figures S1-S16**

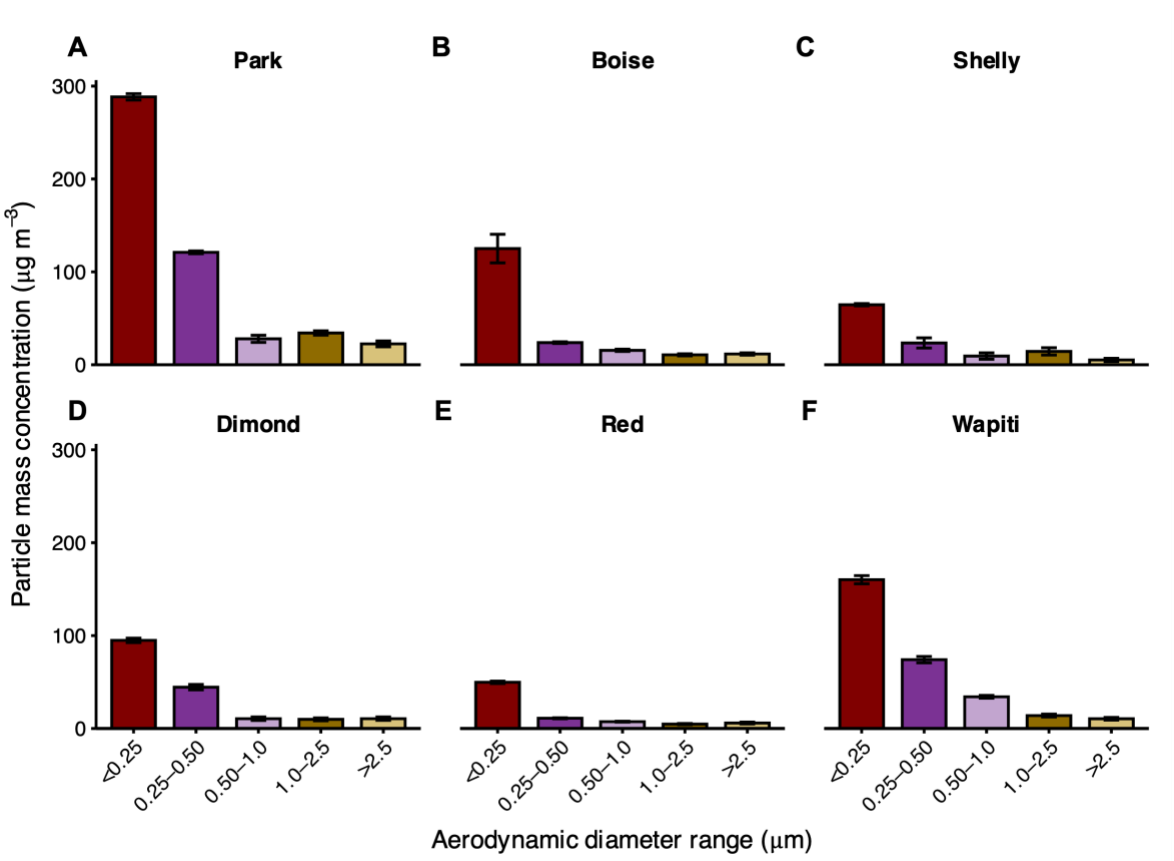

871

872 **fig. S1. Change in smoke PM mass across aerodynamic diameter ranges collected on each impactor stage.** Middle
873 Fork Complex Fire data follow the same trend and are not shown. Masses from the remaining fires were below the detection
874 limit of the balance.

875

876

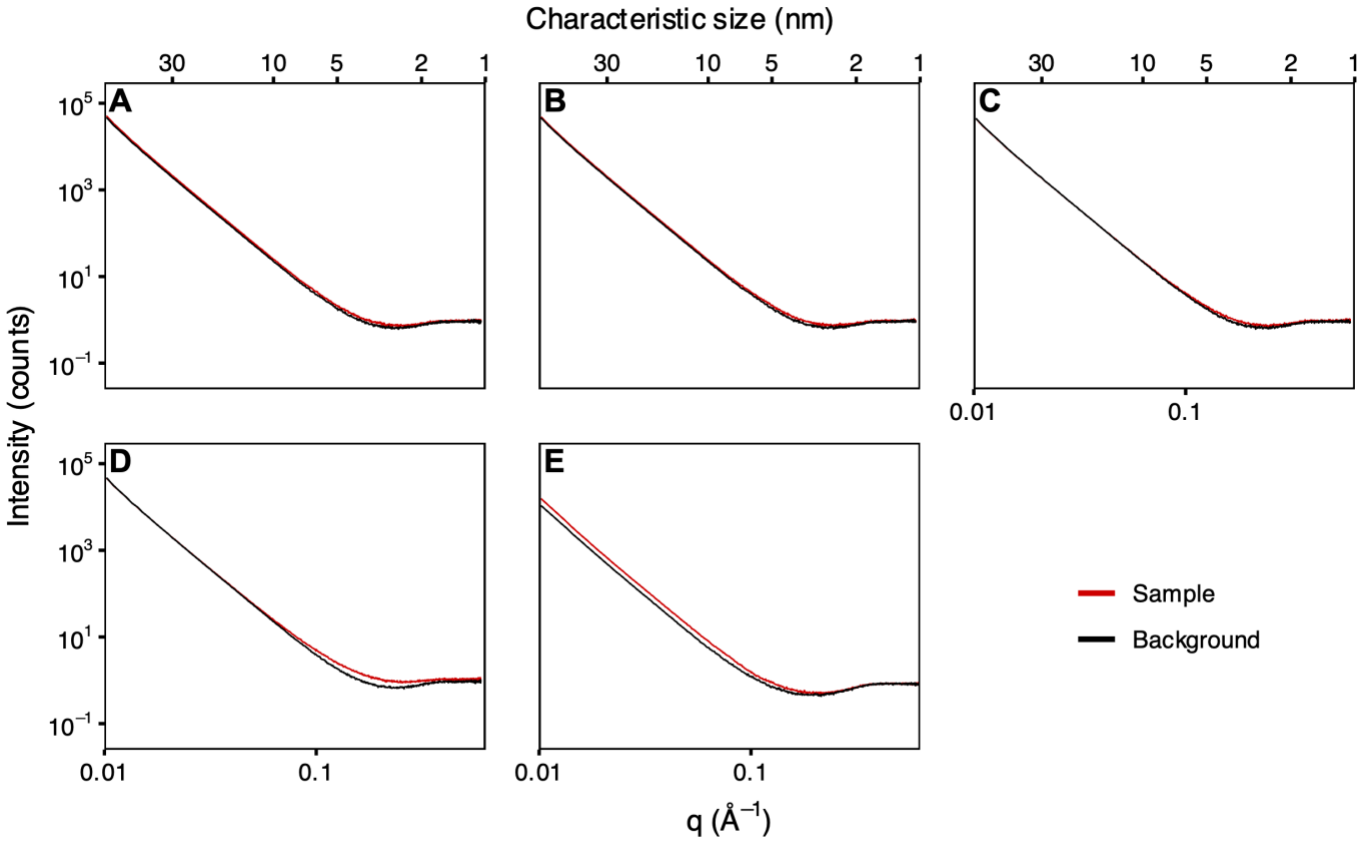

fig. S2. Small-angle X-ray scattering (SAXS) profiles for particles collected on different aerodynamic diameters. (A) >2.5 μm, (B) 2.5-1.0 μm, (C) 1.0-0.50 μm, (D) 0.5–0.25 μm, and (E) <0.25 μm impactor stages for the Park Fire PM. The upper x-axis indicates the corresponding characteristic particle size range probed by the measurements.

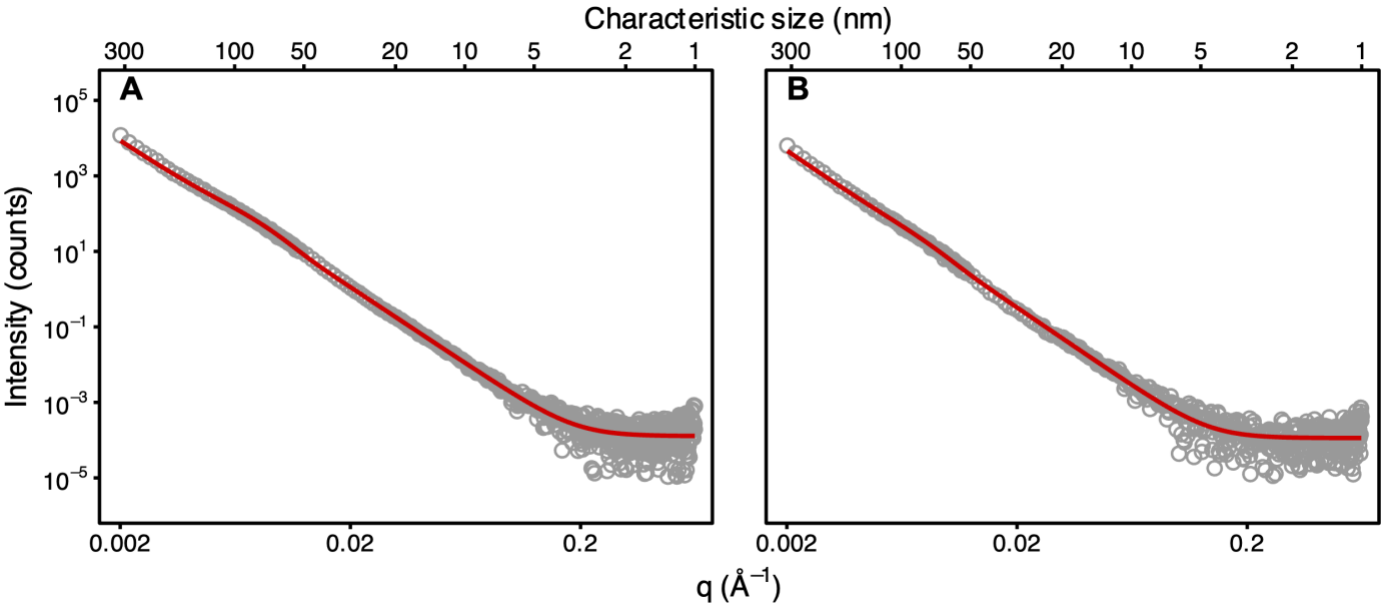

fig. S3. Power-law–subtracted SAXS profiles and corresponding fits (red lines). (A) Park Fire and (B) Boise Fire samples. Average particle size was obtained from reciprocal-space fitting using a Guinier–Porod model, which refines an effective size directly from the scattering pattern. Due to strong particle–particle and particle–filter correlations, a unique real-space size distribution cannot be resolved; instead, the model yields a physically constrained average size that best reproduces the observed intensity decay. Small deviations from this refined size lead to a clear mismatch between the model and data, analogous to misfit in Rietveld refinement.

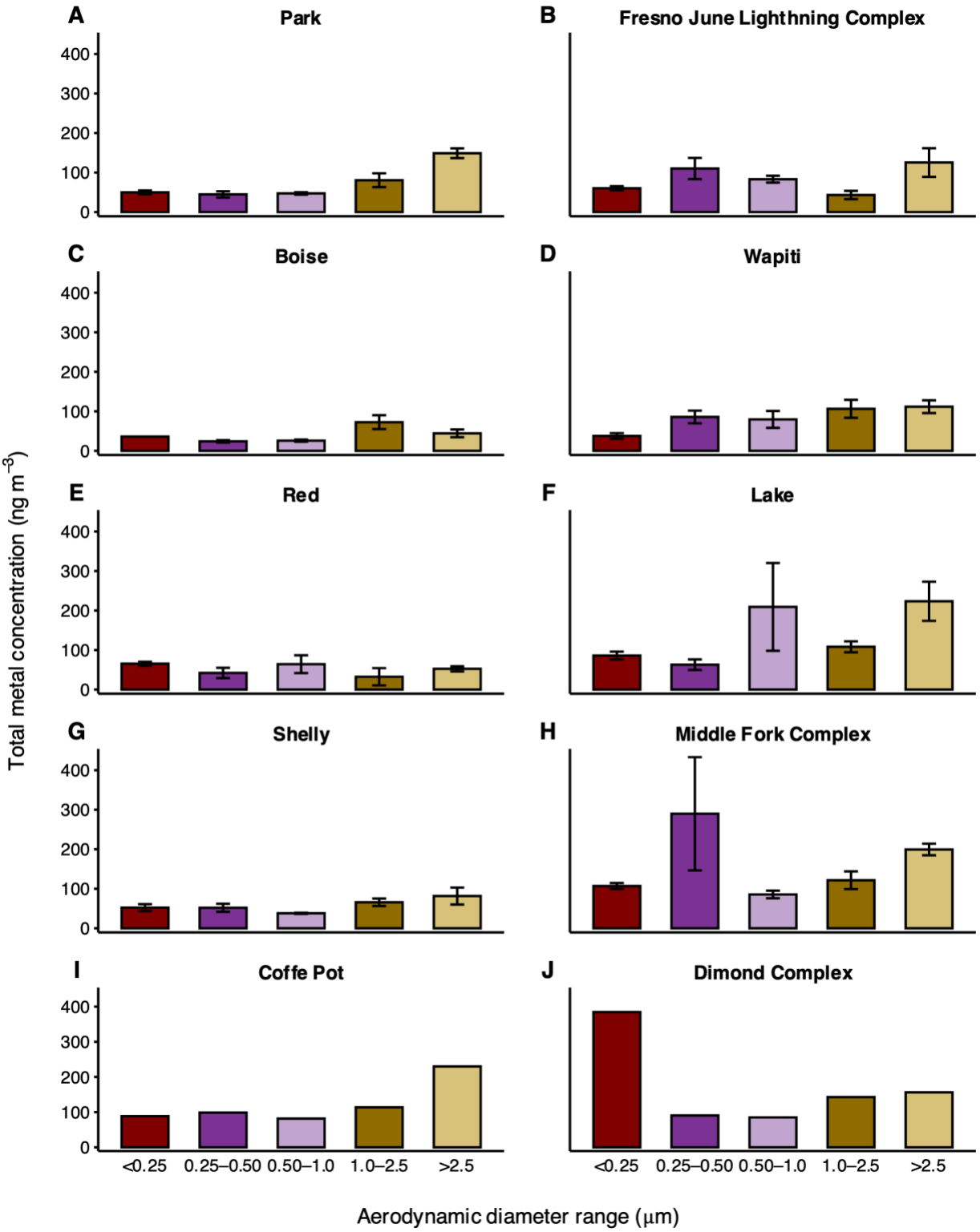

fig. S4. Distribution of total metal concentrations in smoke PM across aerodynamic diameter ranges collected on each impactor stage. Duplicate samples were measured for the Coffee Pot and Dimond Complex fires and Boise fire <0.25 stage; therefore, standard errors are not shown.

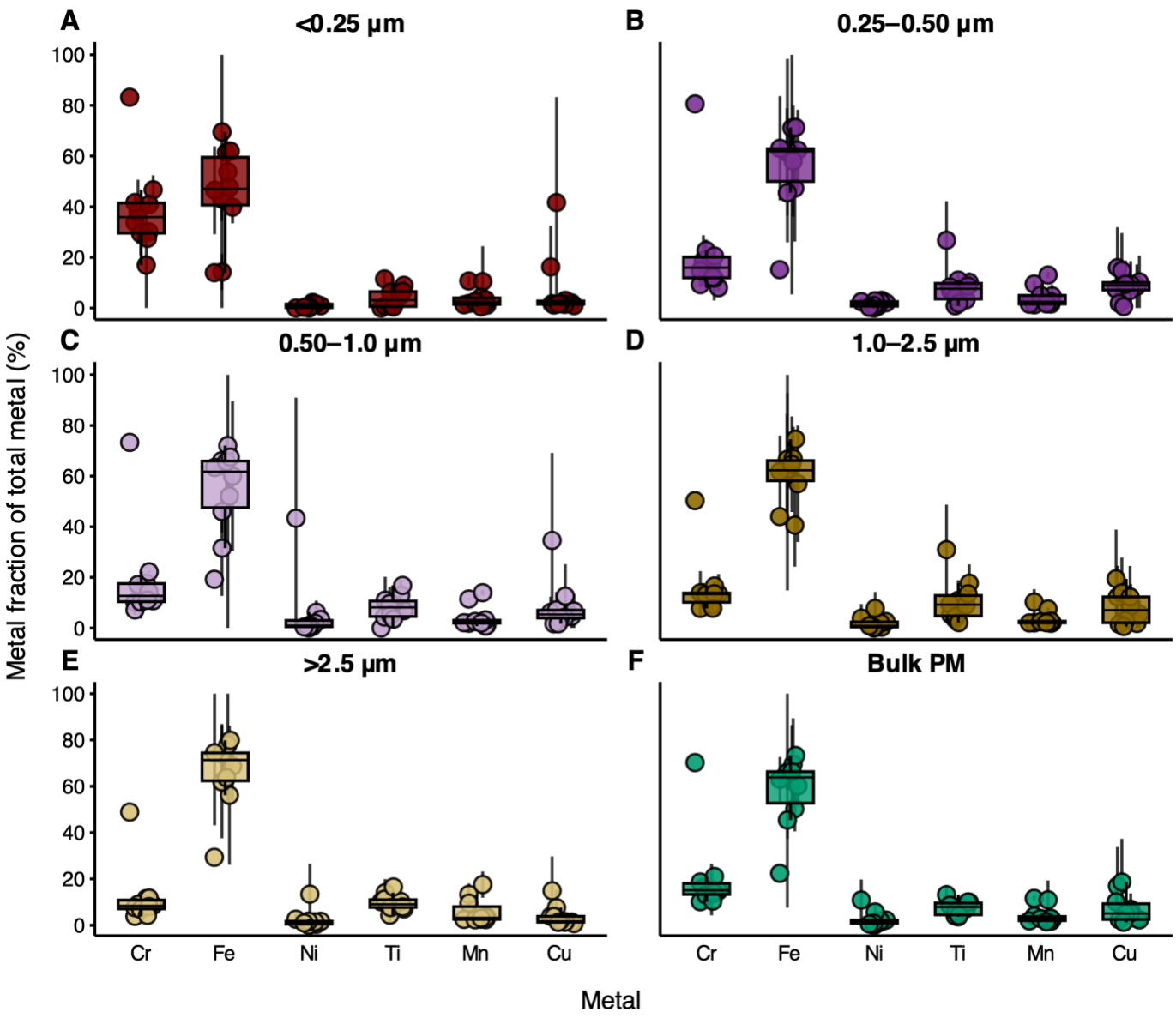

fig. S5. Size-resolved distribution of metals in wildfire smoke particles. Boxplots show the percentage contribution of each metal (Cr, Fe, Ni, Ti, Mn, Cu) to the total metal mass a-e) within each aerodynamic diameter range collected by the cascade impactor, and (f) bulk smoke. The ratio is calculated as the concentration of each metal divided by the sum of all measured metals within the same size fraction.

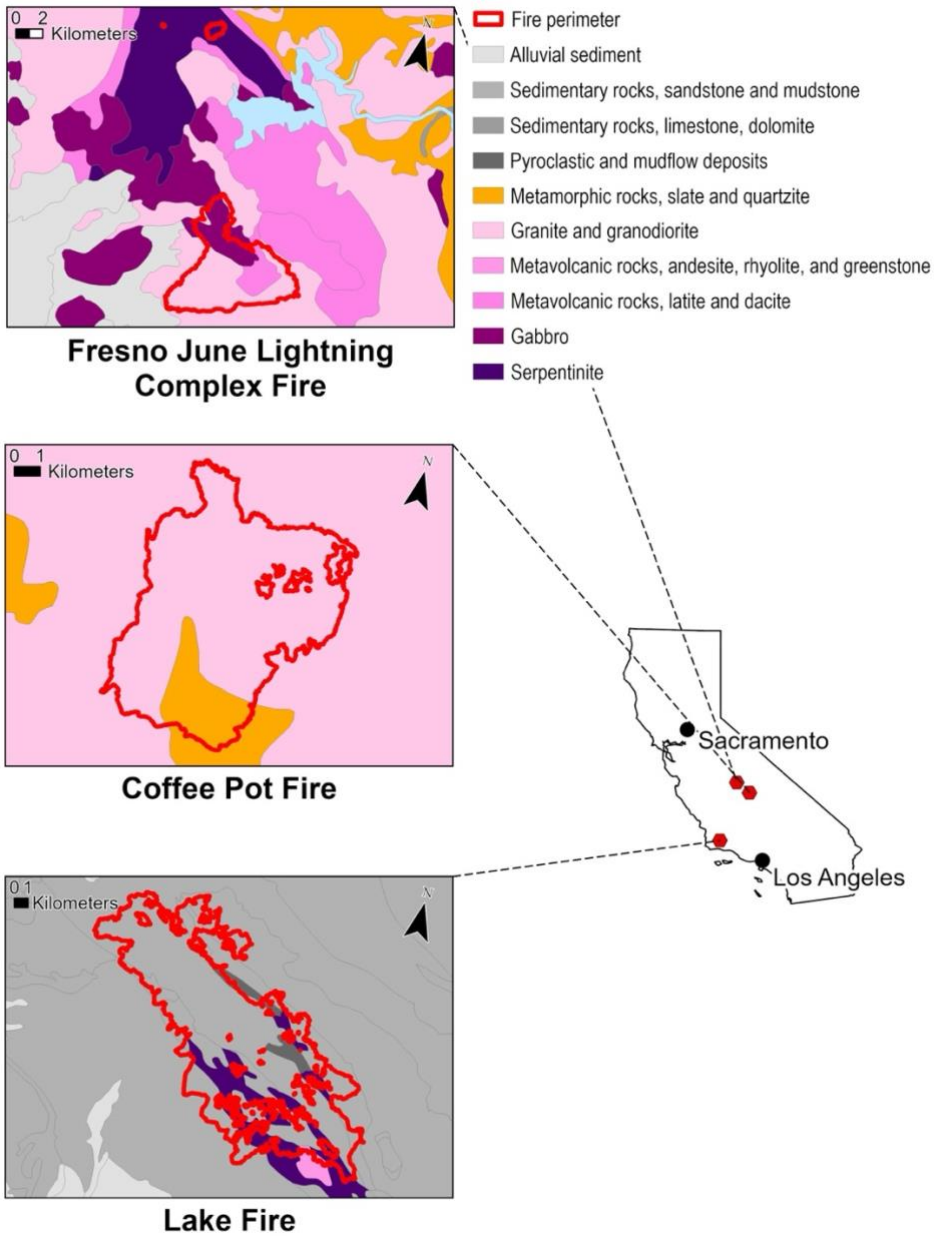

fig. S6A. Simplified geological map of the fire perimeter for the sampled wildfire in southern California. The metal composition increases from top to bottom in the legend.

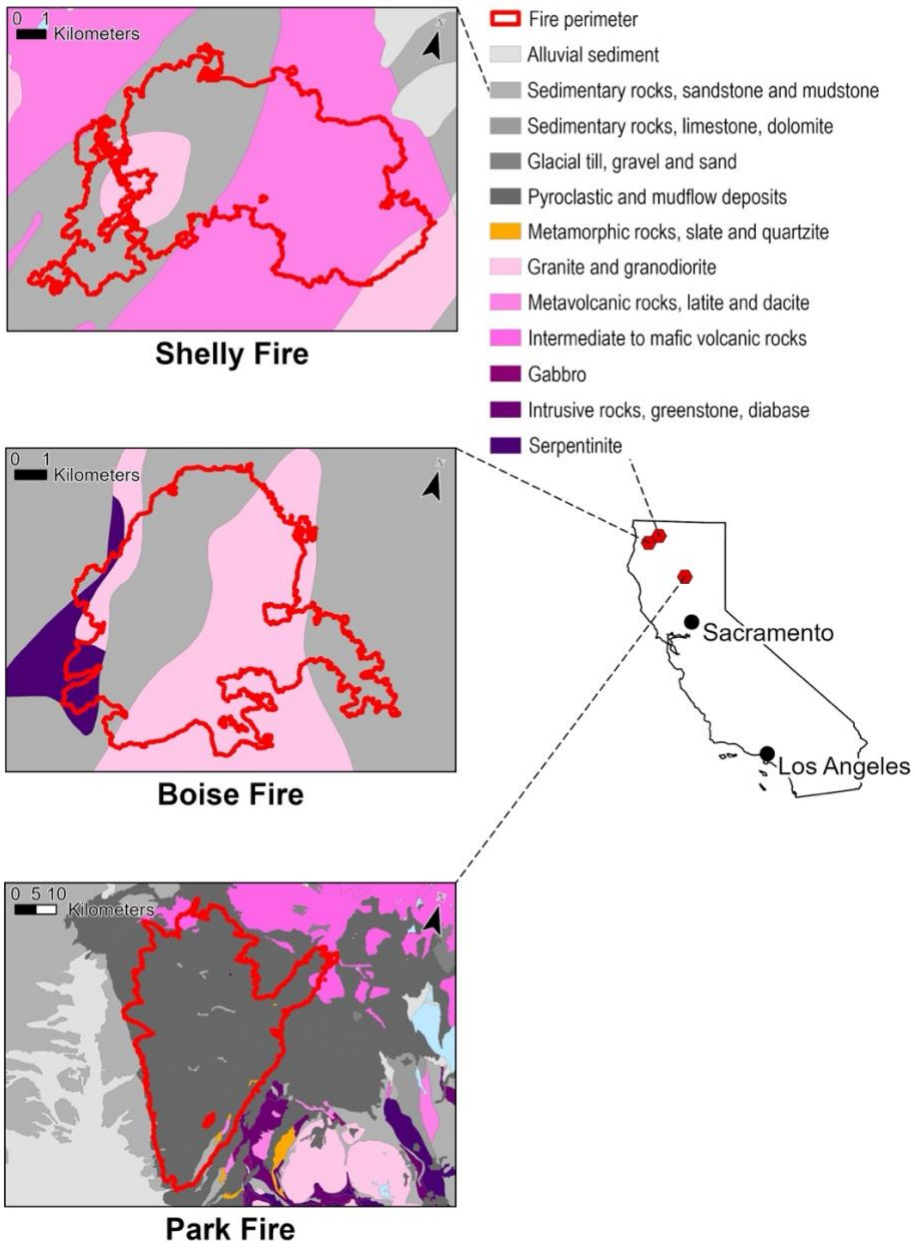

fig. S6B. Simplified geological map of the fire perimeter for the sampled wildfire in northern California.

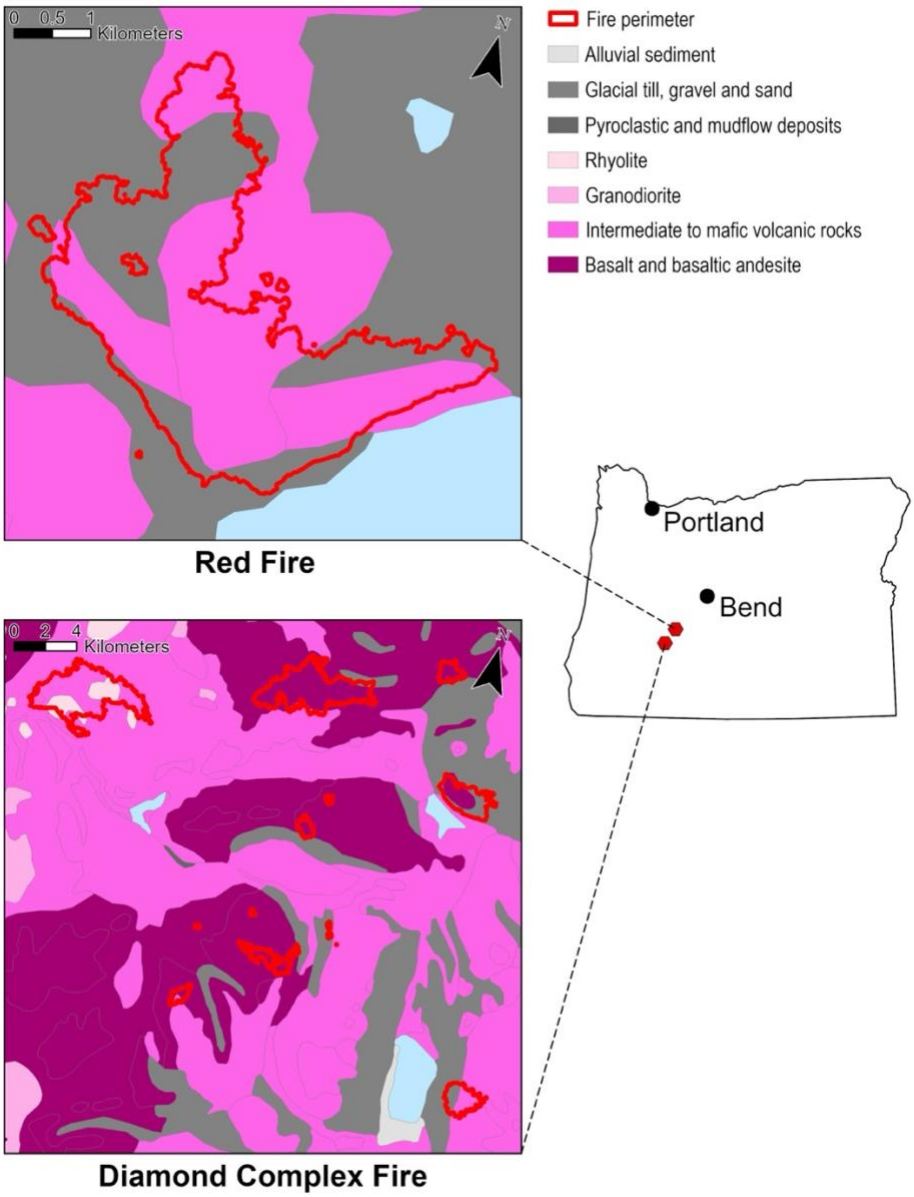

fig. S6C. Simplified geological map of the fire perimeter for the sampled wildfire in Oregon.

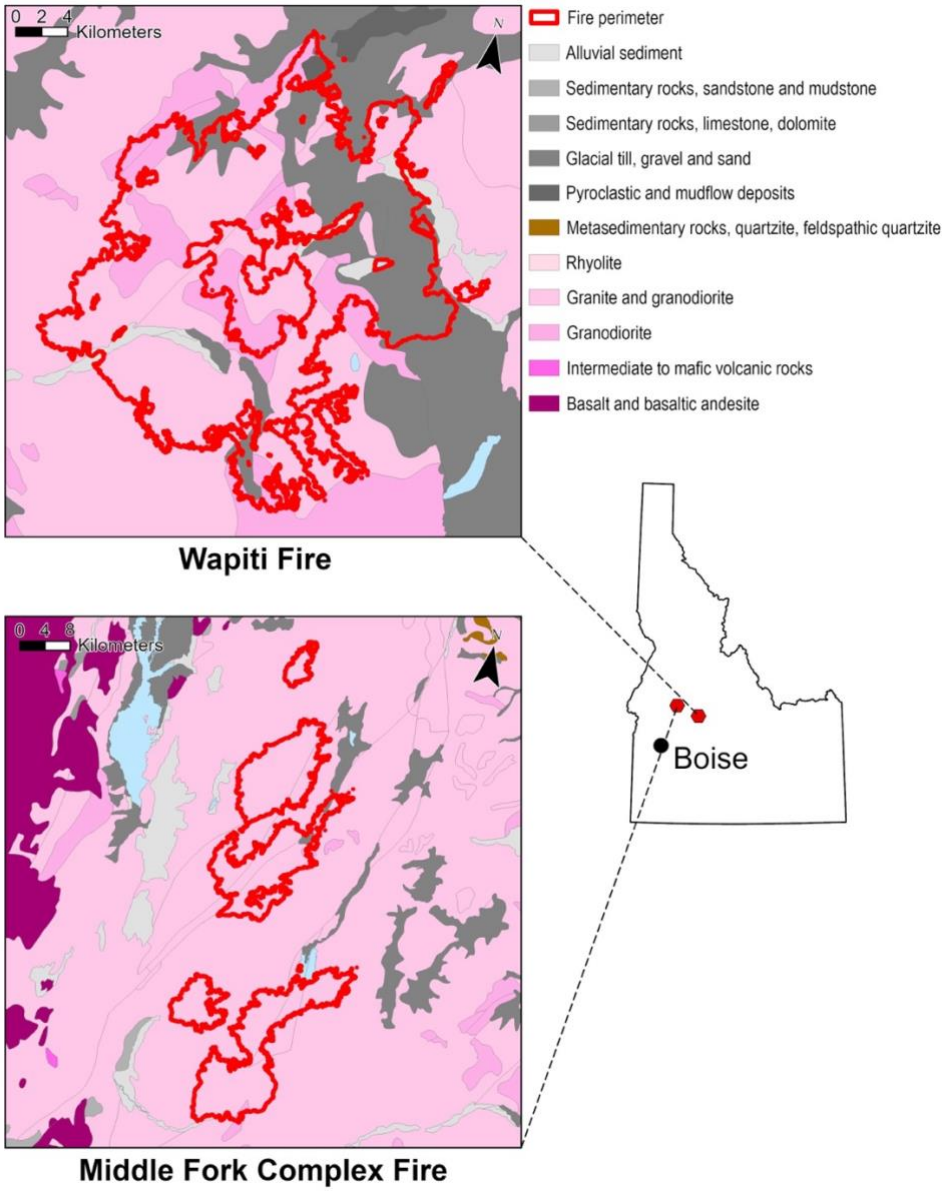

944

945 **fig. S6D. Simplified geological map of the fire perimeter for the sampled wildfire in Idaho.**

946

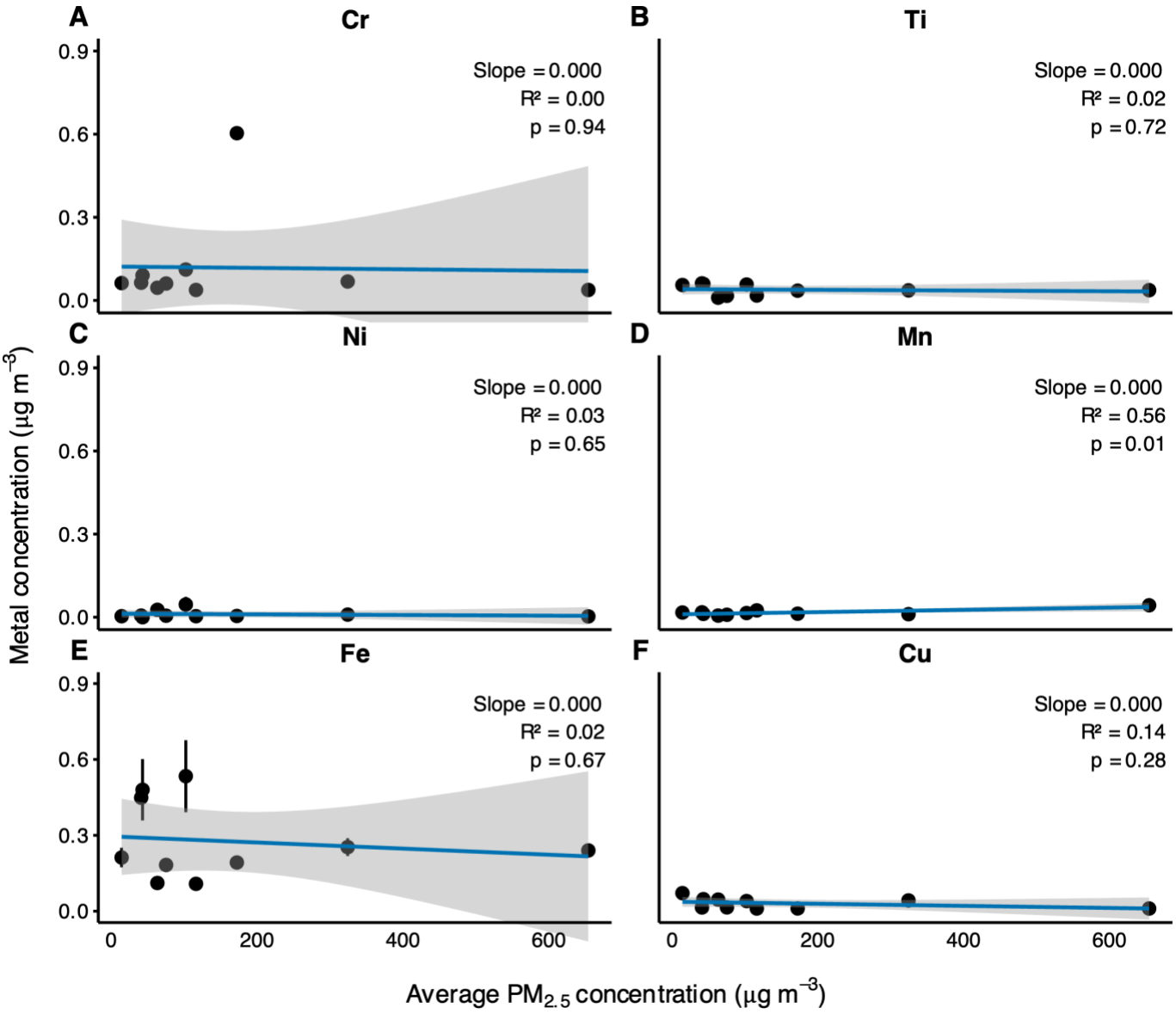

fig. S7. Relationship between metal concentrations (Cr, Ti, Ni, Mn, Fe, and Cu) and average $PM_{2.5}$ concentration across all sampled wildfires.

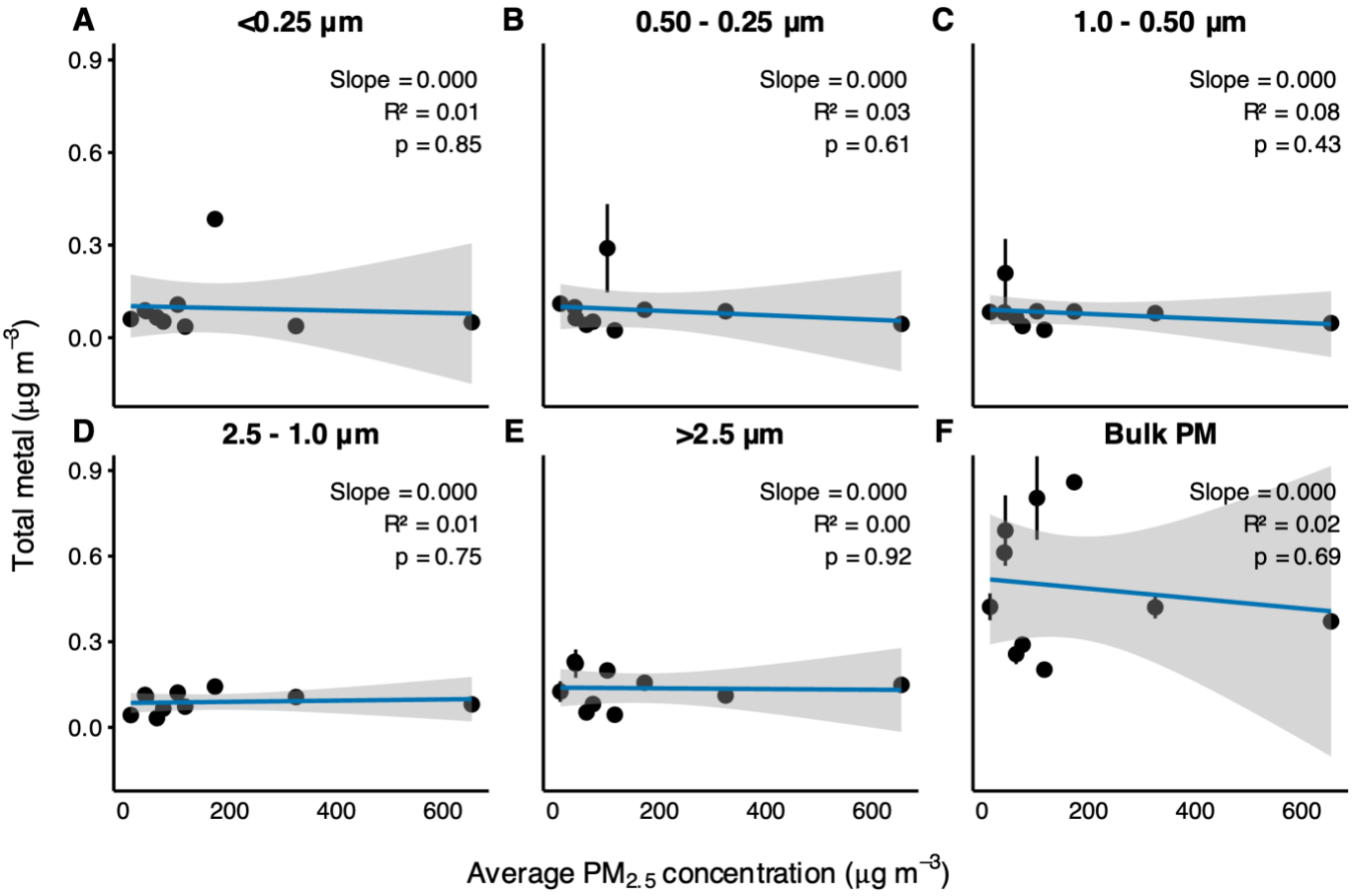

951

952 **fig. S8. Relationship between total metal concentrations and average $PM_{2.5}$ concentration across aerodynamic size**

953 **fractions for all wildfires (n = 10).**

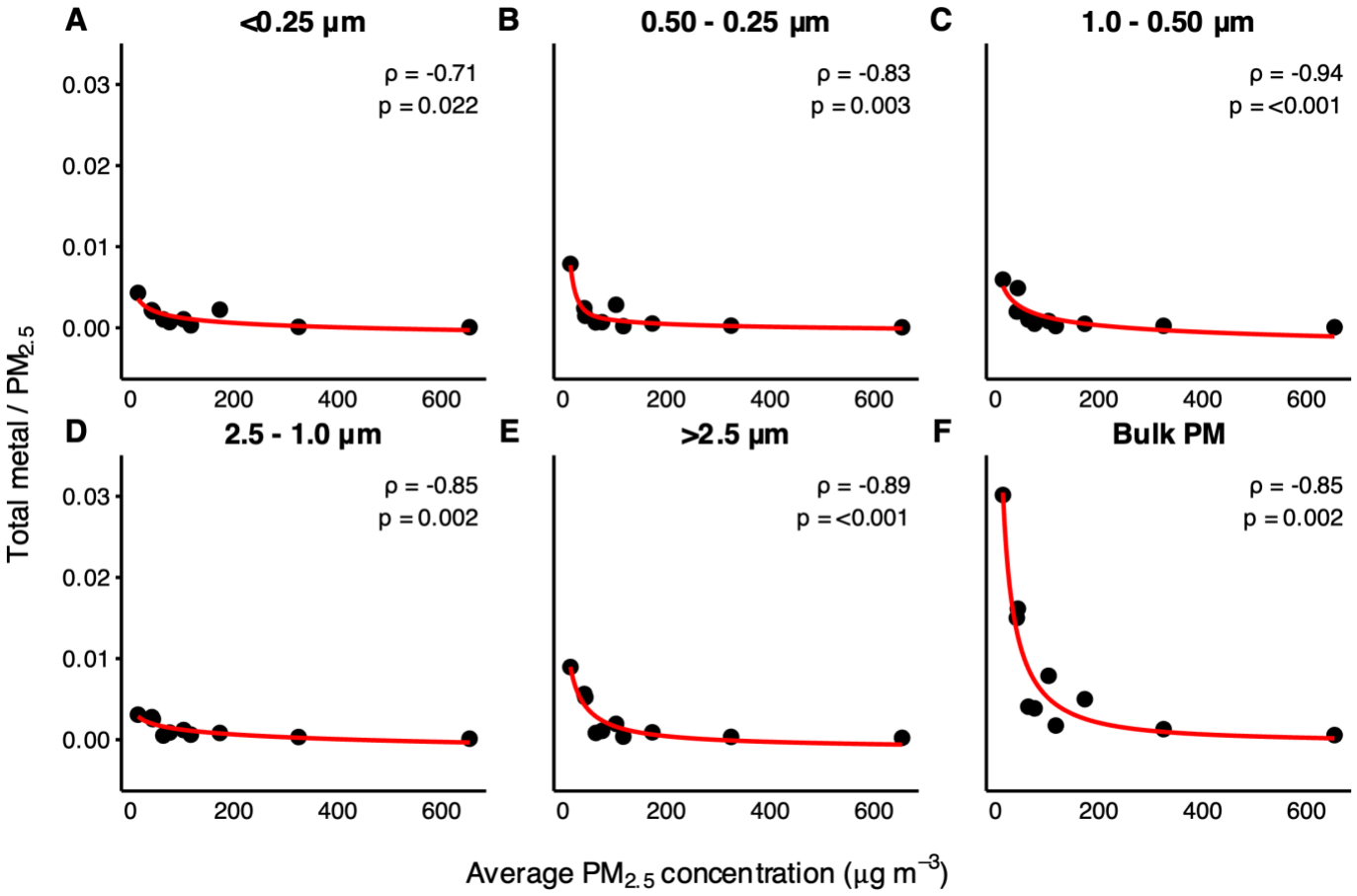

fig. S9. Spearman rank correlations between the ratio of total metal to $PM_{2.5}$ and average $PM_{2.5}$ concentration across aerodynamic size fractions and bulk smoke for all wildfires (n = 10). Values of Spearman's ρ and corresponding p values are shown in each panel. The red curve shows a monotonic smooth fit used only to visualize the overall negative trend.

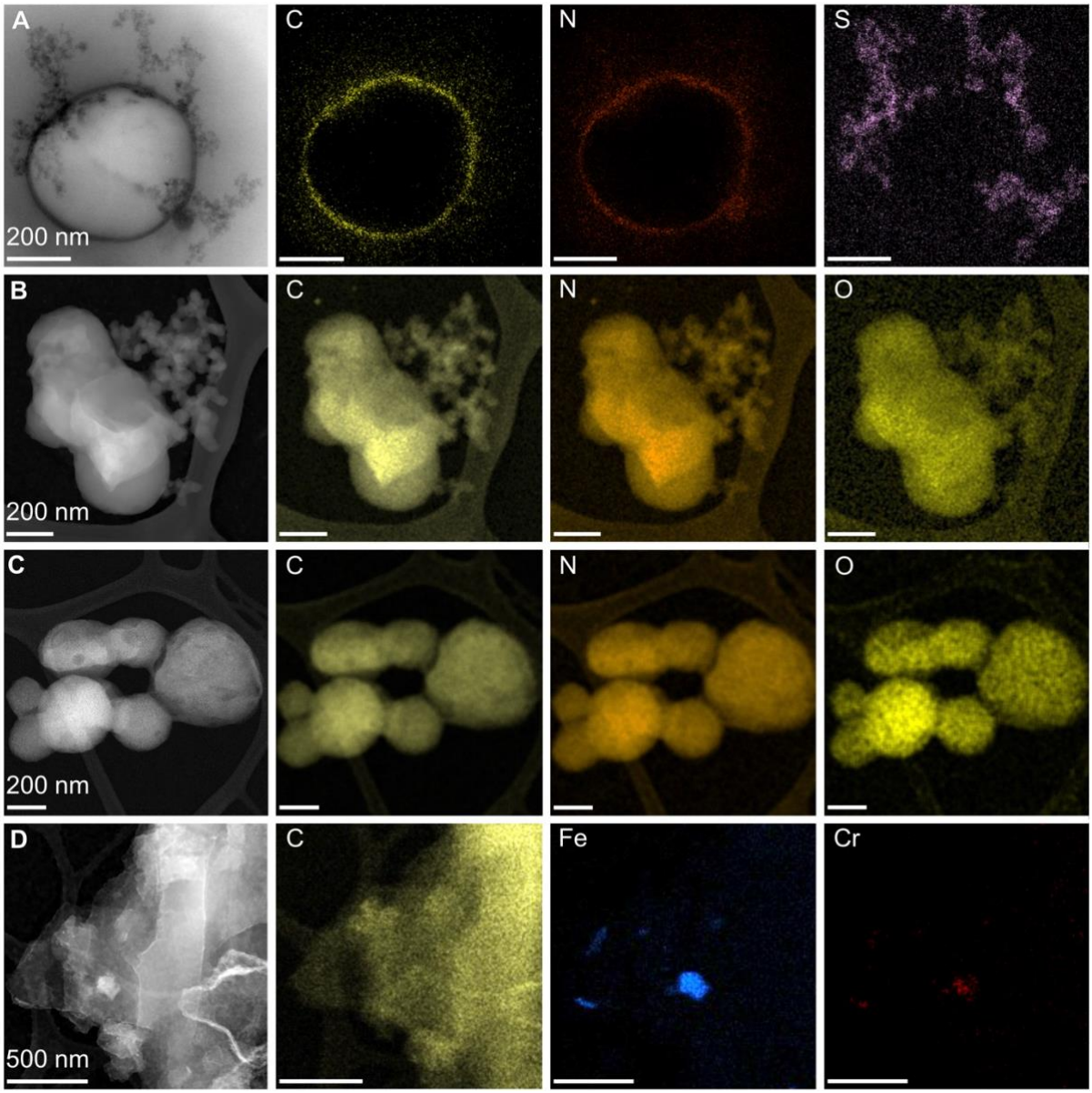

fig. S10. Scanning transmission electron microscopy (STEM) images and corresponding elemental maps of particles collected on submicron impactor stages. (A) 0.50–0.25 μm stage from the Park Fire, showing a large organic particle surrounded by chain aggregates of organic nanoparticles, (B) <0.25 μm stage from the Shelly Fire, showing aggregated organic nanoparticles (C) <0.25 μm stage from the Shelly Fire, showing spherical organic particles with diameters of a few hundred nanometers (D) 0.50–0.25 μm stage from the Shelly Fire, showing Fe- and Cr-containing nanoparticles embedded within an organic matrix.

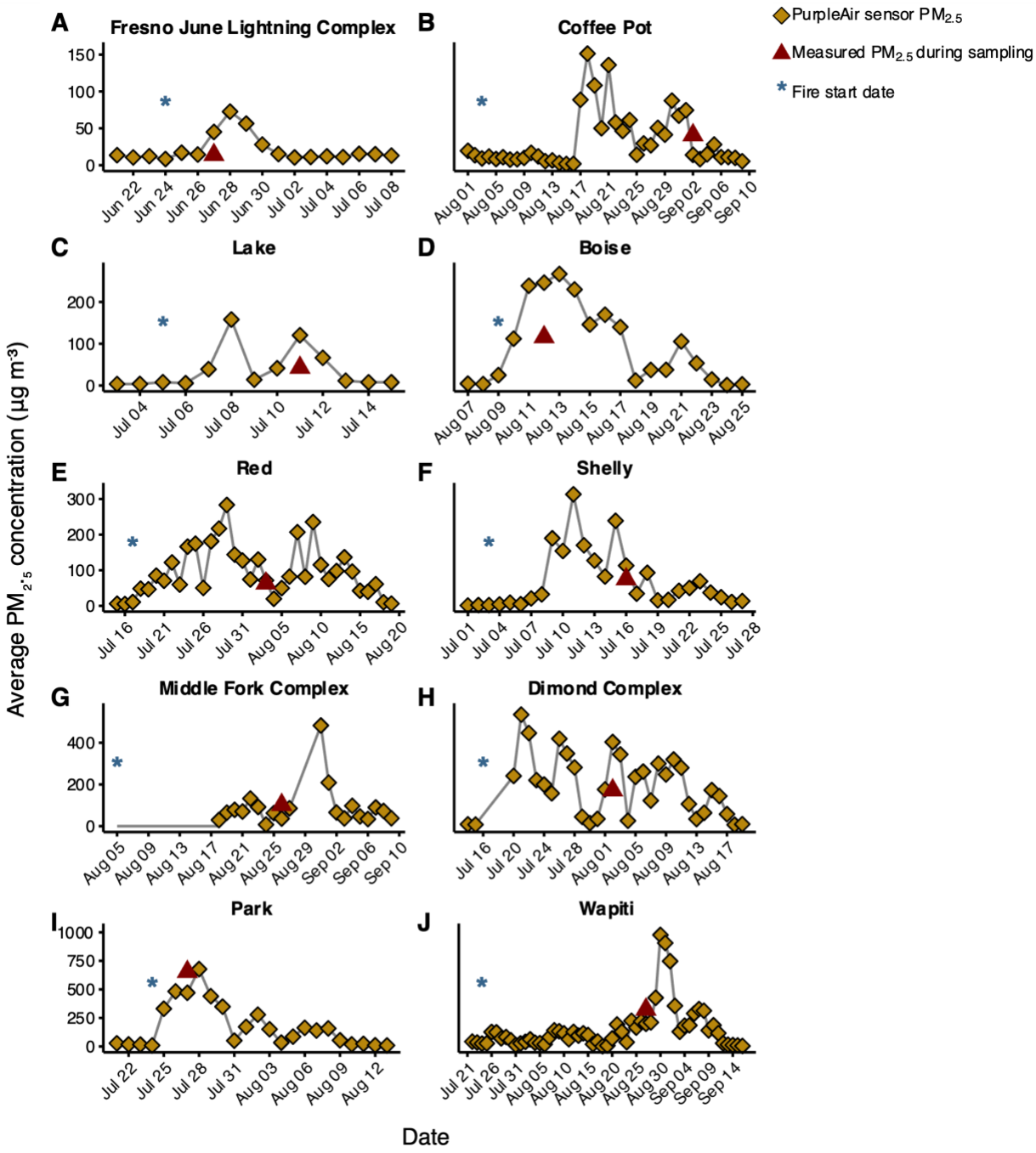

fig. S11. Temporal variation in smoke $PM_{2.5}$ concentrations for each wildfire, including wildfire start date, sampling dates, and $PM_{2.5}$ concentrations measured during sample collection. The figure shows that $PM_{2.5}$ concentrations during sampling were elevated relative to baseline conditions. PurpleAir data represent daily average $PM_{2.5}$ concentrations, whereas measured $PM_{2.5}$ values reflect averages over sample collection periods of up to 7 hours, which explains the differences between the two on some sampling days. The PurpleAir sensor did not report any data from August 5–17 for the Middle Fork Complex Fire.

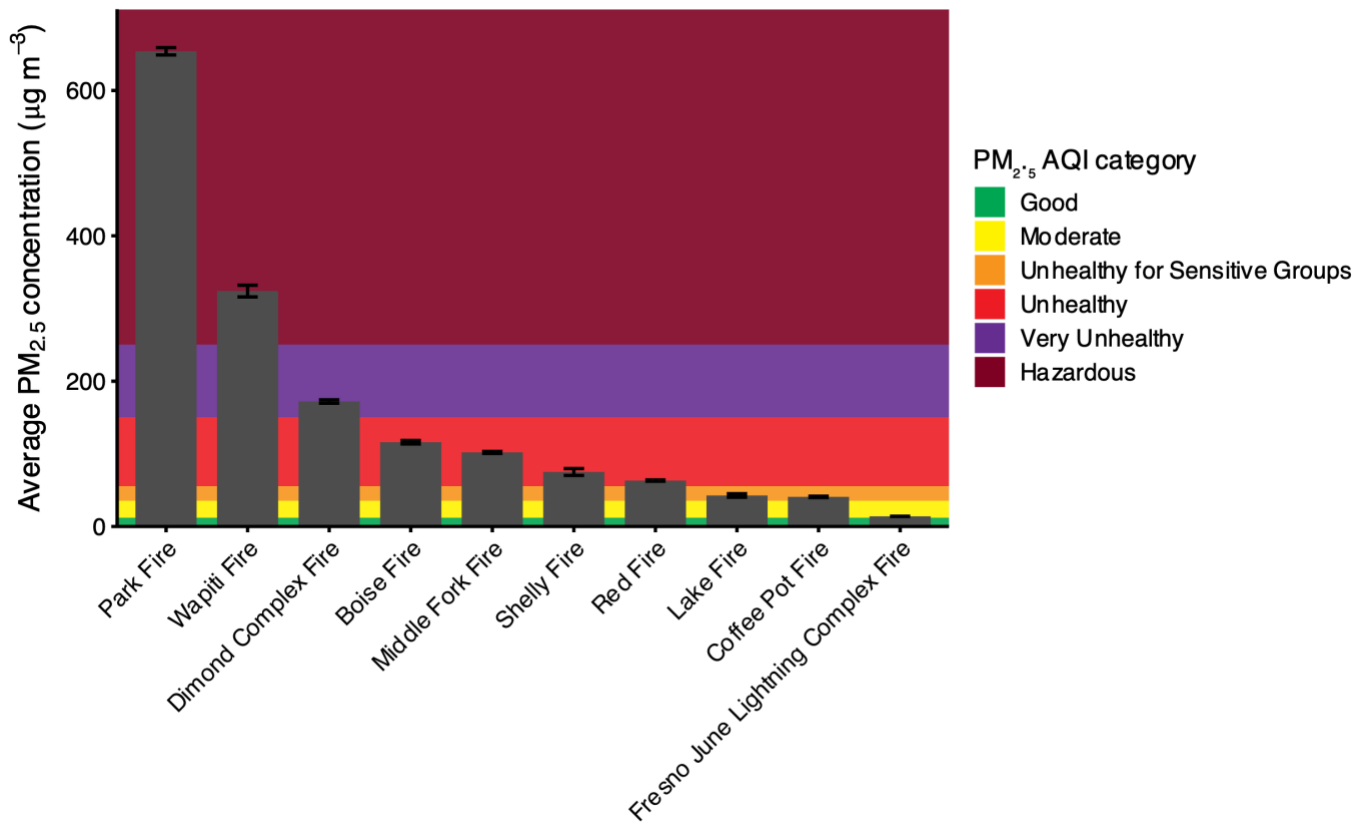

fig. S12. $PM_{2.5}$ concentrations in wildfire smoke across sampled wildfires during sample collection, with AQI categories indicated by color coding.

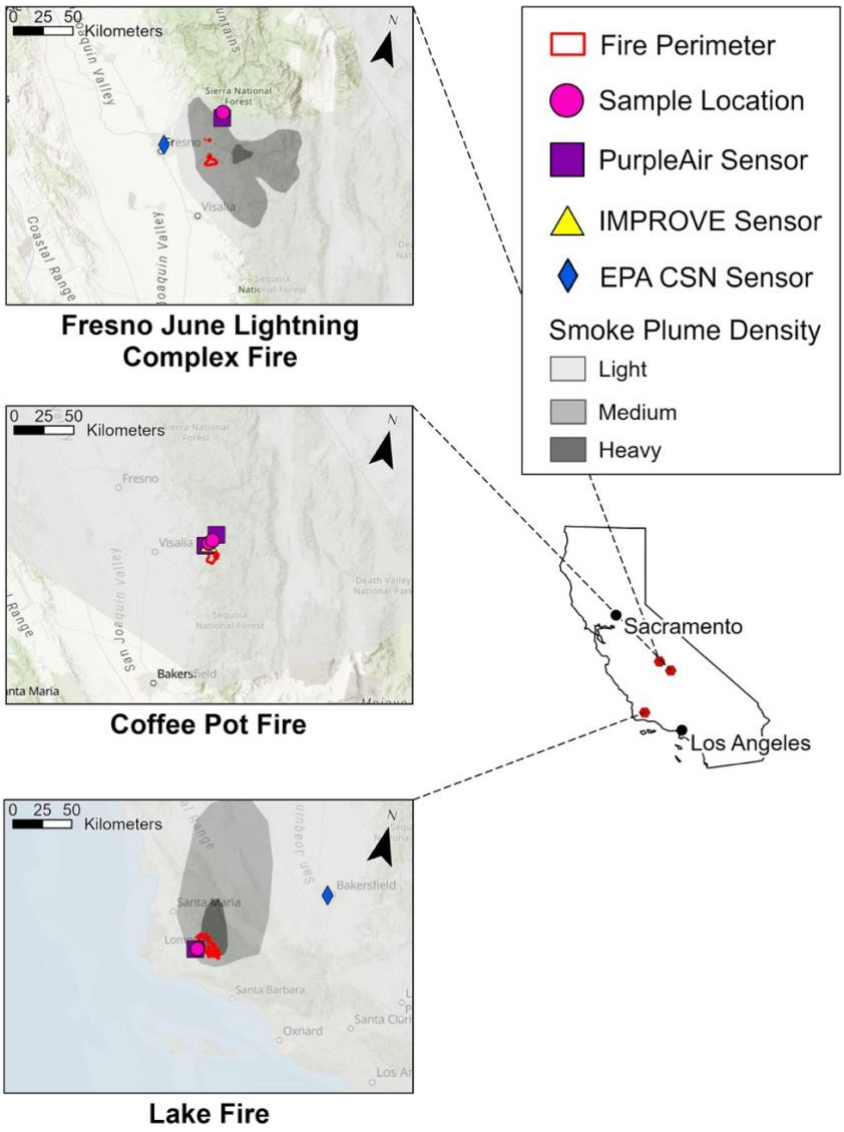

fig. S13A. Smoke plume extent over sampling locations for sampled wildfires in southern California. Fire perimeters and smoke plume density are shown relative to sampling locations, demonstrating that samples were collected while the sites were within active smoke plumes. Locations of PurpleAir sensors used to guide sample-site selection, as well as nearby CSN and IMPROVE monitoring stations, are shown.

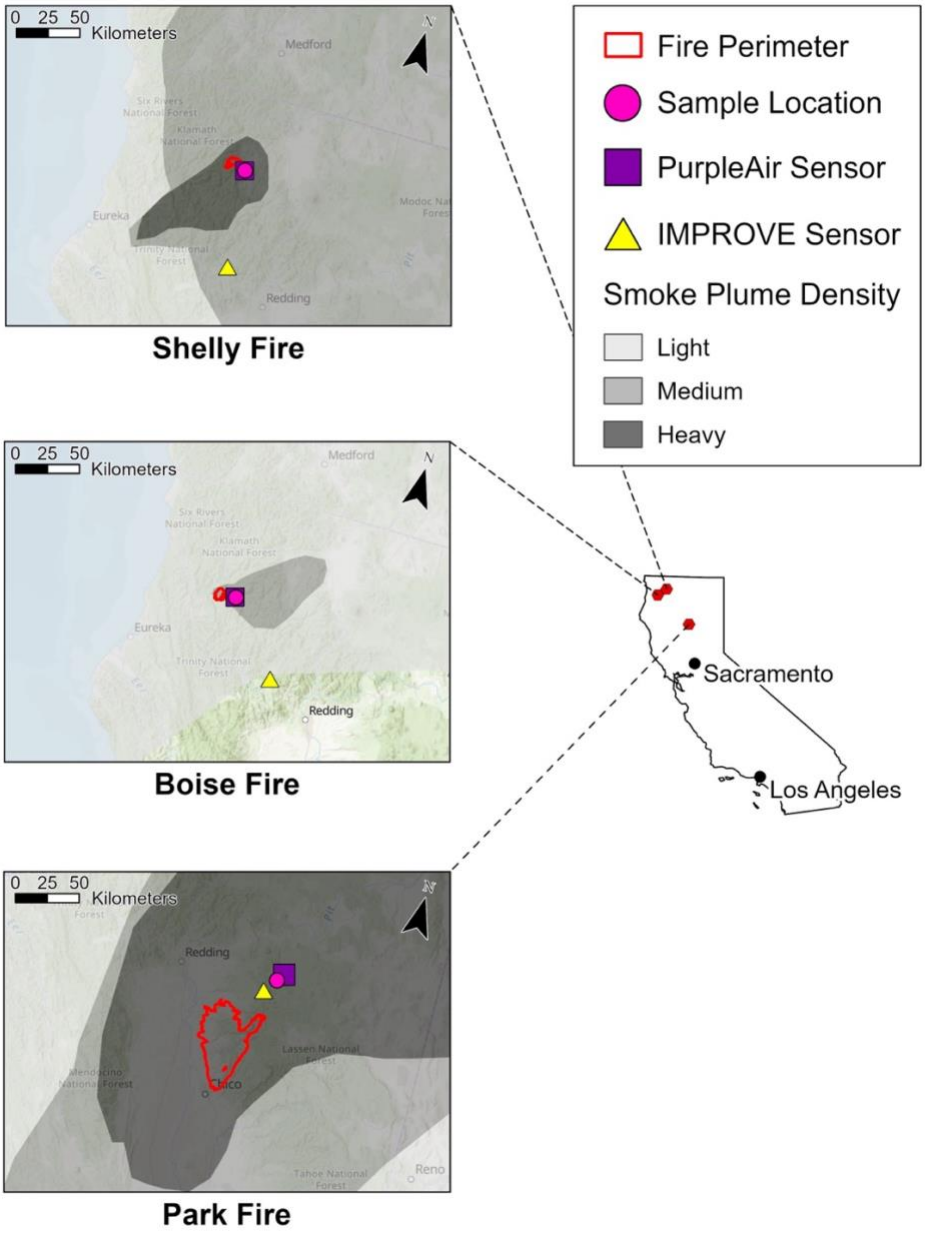

991

992 **fig. S13B. Smoke plume extent over sampling locations for sampled wildfires in northern California.**

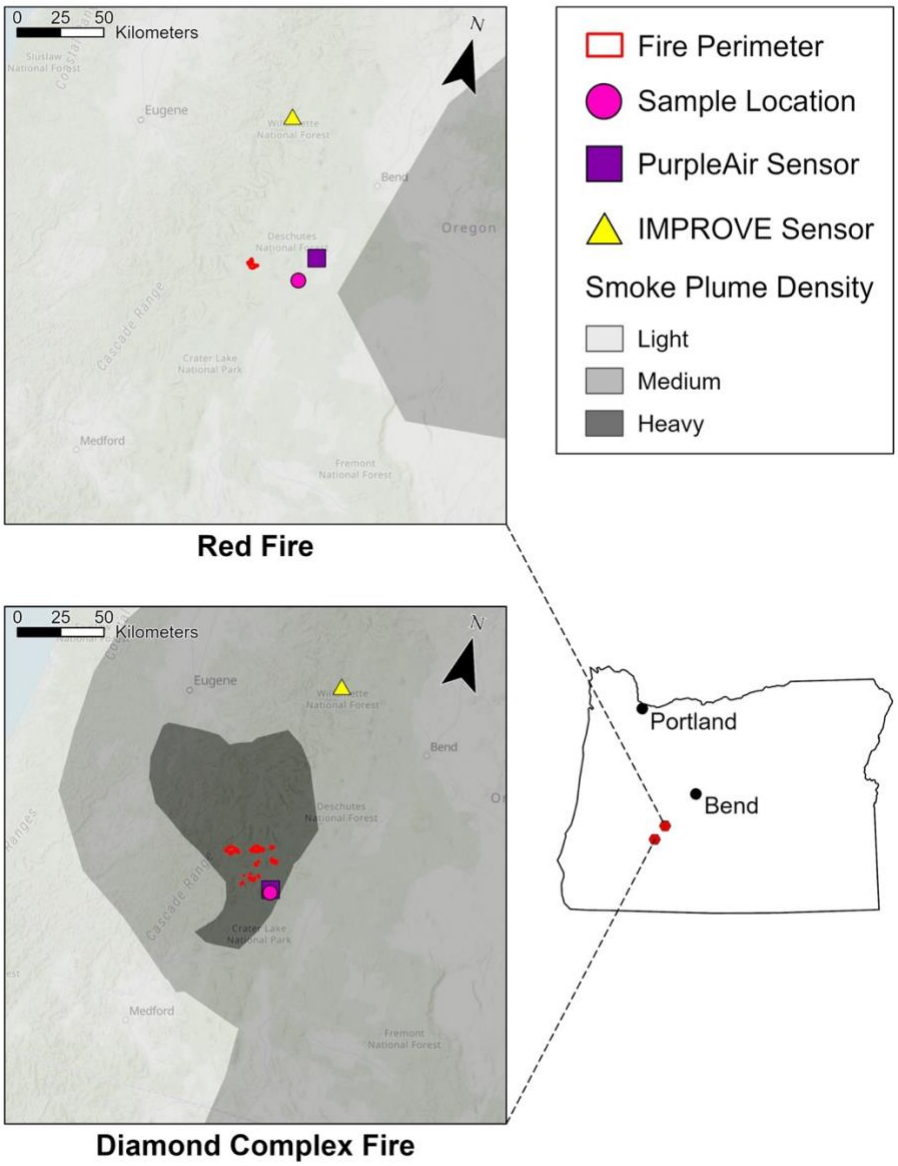

993

994 **fig. S13C.** Smoke plume extent over sampling locations for sampled wildfires in Oregon.

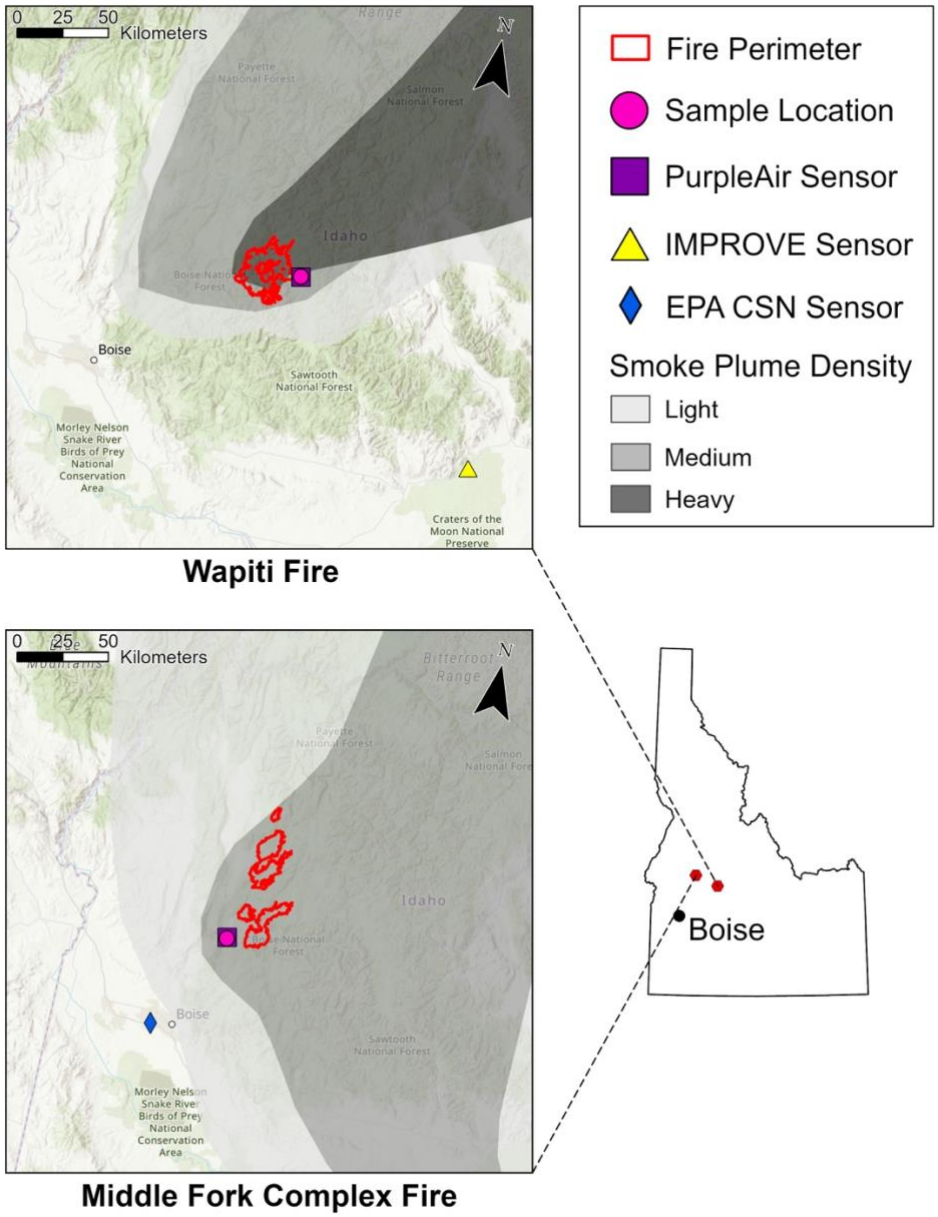

fig. S13D. Smoke plume extent over sampling locations for sampled wildfires in Idaho.

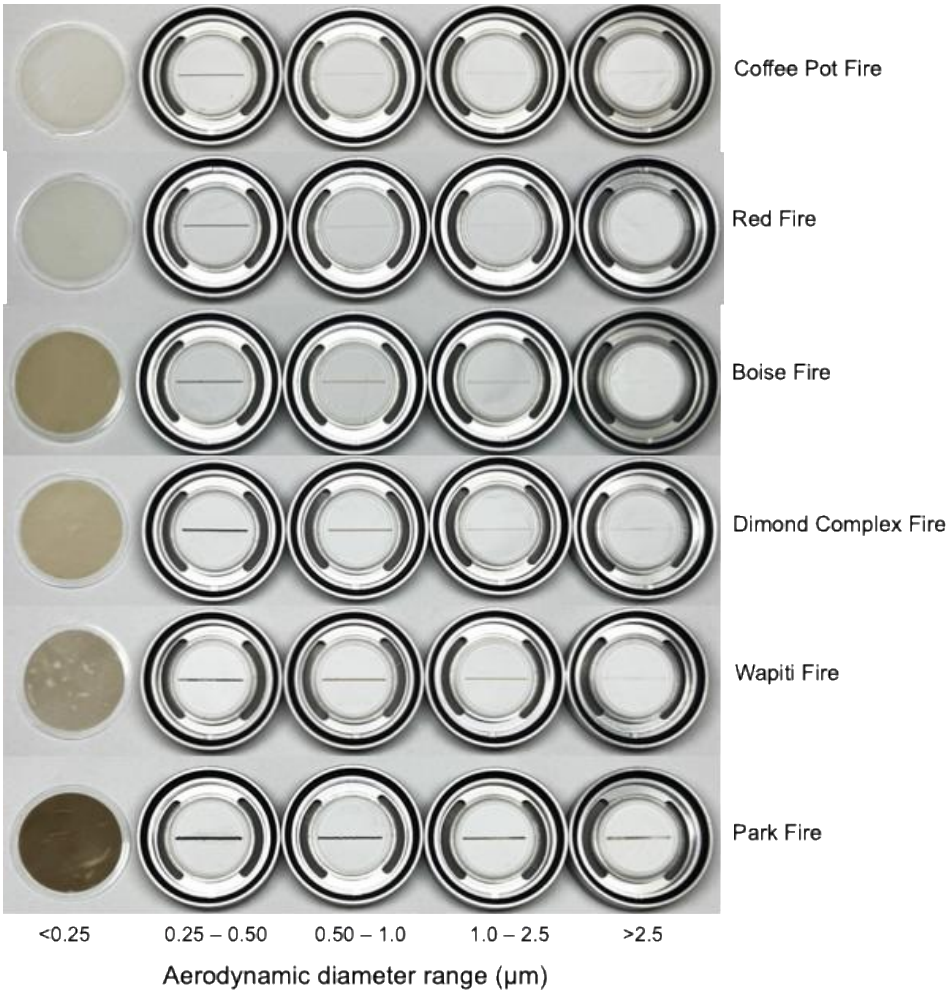

fig. S14. Photographs of smoke particles collected on filters for selected wildfires. Particles are deposited as a line after passing through the narrow slit of each impactor stage. The remaining particles are collected on the final collection stage (<0.25 µm), which has a different configuration. From right to left, particle loading on the filters increases with decreasing aerodynamic diameter range. Filters corresponding to >2.5, 2.5–1.0, 1.0–0.50, and 0.50–0.25 µm stages are shown mounted on their impactor disks, whereas the <0.25 µm collection filter is removed from the impactor for clearer visualization.

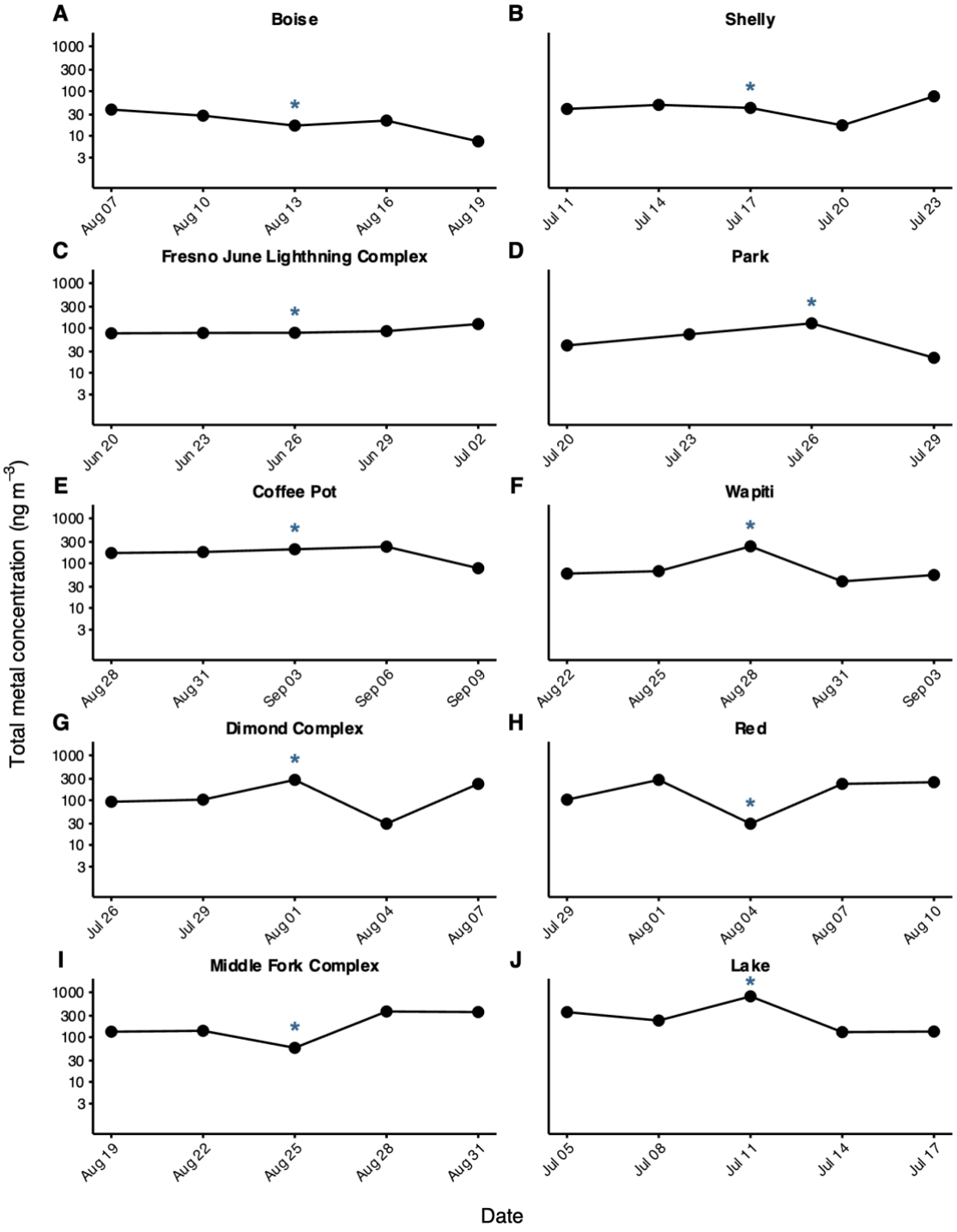

fig. S15. Temporal variation in total metal concentrations for each wildfire before and after the sample collection date (indicated by a blue star). Total metal includes Cr, Ti, Ni, Mn, Fe, and Cu. Other metals were excluded because of their extremely low concentration in our collected samples. No data were reported for the six days following the sample collection date for the Park Fire.

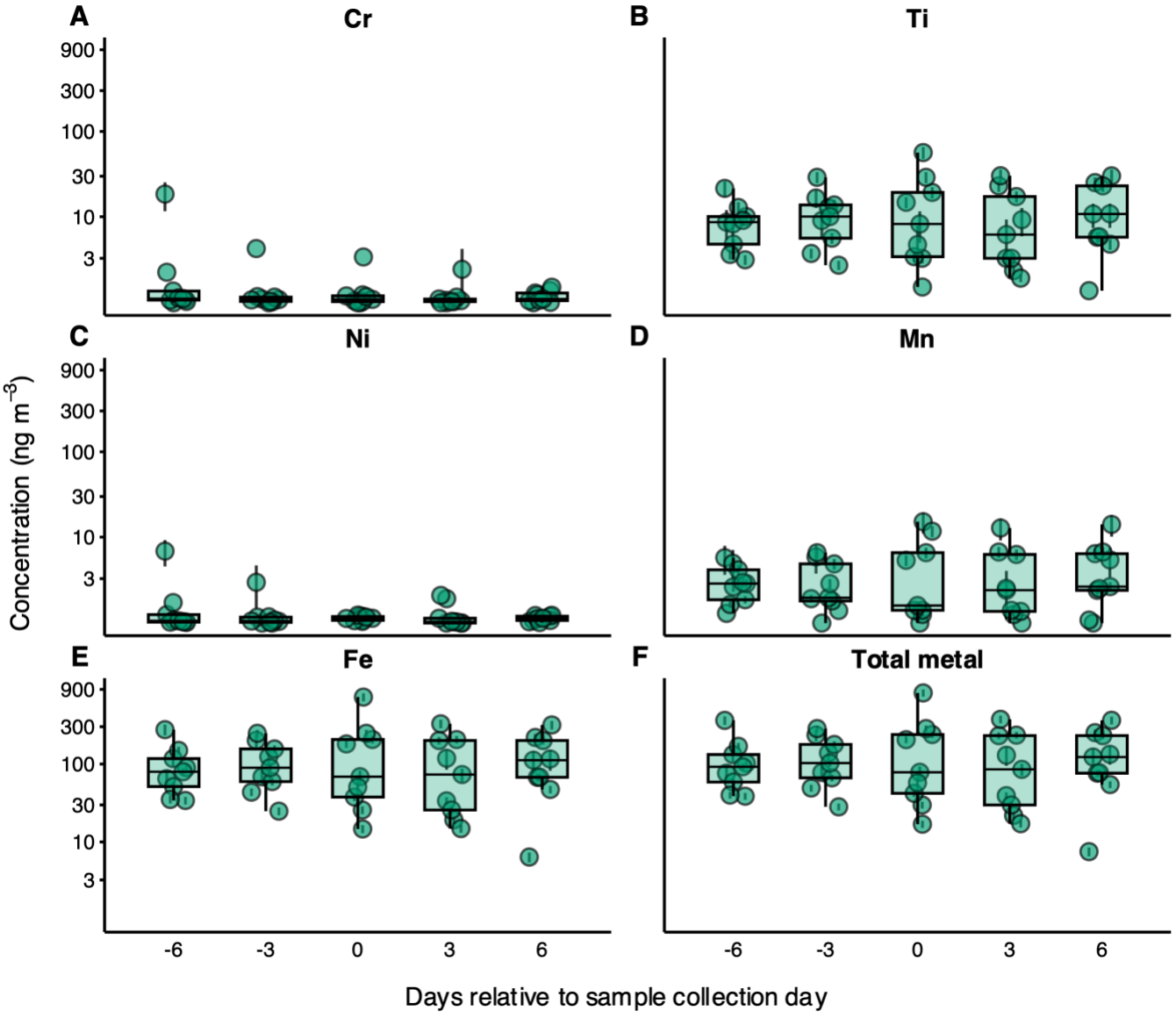

fig. S16. Temporal distribution of smoke metal content for each wildfire (n = 10) before and after the sample collection date (day 0). The actual dates are provided in fig. S15. Error bars represent standard error, where available, and are shown only when the lower bound remained positive (SE > 0) and the measured value was ≥1 ng m^{-3}; points are shown for all measurements.

table S1. Geological classification, layer scoring, and acreage used to compute the Geology Composition Index for each wildfire.

Wildfire	Geologic Layers	Geology classification	Layer Scores	Layer Acres	Total Fire Acres	Geological Composition Score
Boise	Granites and Granodiorite	Felsic to intermediate	2.5	6539	12912	1.96
	Sedimentary rocks, sandstone and mudstone	Sedimentary low metal	1.0	5802		
	Serpentinite	Ultramafic	5.5	571		
Coffee Pot	Granite and granodiorite	Felsic to intermediate	2.5	12061	14103	2.28
	Metamorphic rocks, slate and quartzite	Metamorphic low metal	1.0	2042		
Diamond	Basalt and basaltic andesite	Mafic	5.0	5284	11047	4.06
	Volcanic rocks	Intermediate to mafic	4.5	3620		
	Glacial till, gravel and sand	Sedimentary low metal	1.0	1094		
	Rhyolite	Felsic	1.0	1049		
Fresno June Lightning	Granite and granodiorite	Felsic to intermediate	2.5	6387	10640	3.36
	Gabbro	Mafic	5.0	2400		
	Metavolcanic rocks, latite and dacite	Intermediate	4.0	1581		
	Serpentinite	Ultramafic	5.5	272		
Lake	Sedimentary rocks, sandstone and mudstone	Sedimentary low metal	1.0	32154	38612	1.75
	Serpentinite	Ultramafic	5.5	6270		
	Metavolcanic rocks, andesite, rhyolite, and greenstone	Intermediate	4.0	188		
Middle Fork	Granodiorite	Felsic to intermediate	2.5	134618	136017	2.48
	Alluvial sediment	Sedimentary low metal	1.0	130		
	Glacial till, gravel and sand	Sedimentary low metal	1.0	1240		
	Water and ice	Water/Ice	-	29		
Park	Pyroclastic and mudflow deposits	Sedimentary low metal	1.0	411907	429602	1.07
	Sedimentary rocks, sandstone and mudstone	Sedimentary low metal	1.0	7165		
	Volcanic rocks	Intermediate to mafic	4.5	8041		

	Metamorphic rocks, slate and quartzite	Metamorphic low metal	1.0	1428		
	Metavolcanic rocks, latite and dacite	Intermediate	4.0	938		
	Alluvial sediment	Sedimentary low metal	1.0	12		
	Intrusive rocks, greenstone, diabase	Mafic	5.0	111		
Red	Volcanic rocks	Intermediate to mafic	4.5	1818	2994	3.13
	Glacial till, gravel and sand	Sedimentary low metal	1.0	1176		
Shelly	Metavolcanic rocks, latite and dacite	Intermediate	4.0	7656	15520	2.68
	Sedimentary rocks, sandstone and mudstone	Sedimentary low metal	1.0	5845		
	Granite and granodiorite	Felsic to intermediate	2.5	2019		
Wapiti	Granodiorite	Felsic to intermediate	2.5	89977	129062	2.05
	Pyroclastic and mudflow deposits	Sedimentary low metal	1	710		
	Alluvial sediment	Sedimentary low metal	1	4125		
	Glacial till, gravel and sand	Sedimentary low metal	1.0	34238		
	Water and ice	Water/Ice	-	12		

table S2. Summary information for the wildfires from which smoke samples were collected.

Wildfire	State	Fire center coordinates (latitude, longitude)	Date	Time	Sampling location distance from the wildfire center (km)	Speciation sensor distance from the wildfire center (km)	Vegetation
Lake Fire	California	34.759087 -120.017936	10/07/24	9:05 AM-1:25 PM	11.0	109.3	Forest-Mixed Evergreen (6.9 %) Shrubland/Chaparral (59.3 %) Grassland/Herbaceous (30.3 %) Other (3.57 %)
Coffee Pot Fire	California	36.381688 -118.764446	02/09/24	8:25 AM- 8:55 AM 12:30 PM – 17:35 PM	13.5 15.6	77.2	Forest-Mixed Conifer (48.2 %) Forest-Mixed Oak (27.0 %) Forest-Conifer (8.5 %) Shrubland/Chaparral (8.3 %) Grassland/Herbaceous (6.3 %) Other (1.7 %)
Fresno June Lightning Complex Fire	California	36.789497 -119.319469	27/06/24	2:15 PM – 5:15 PM	37.8	40.1	Grassland/Herbaceous (89.2 %) Other (10.8 %)
Boise Fire	California	41.244616 -123.496158	12/8/24	9:10 AM – 15:50 PM	14.5	77.2	Forest-Mixed Evergreen (55.2 %) Forest-Mixed Conifer (34.85 %) Other (9.97 %)
Shelly Fire	California	41.491229 -123.006073	17/07/24	7:00 AM – 12:40 PM	4.3	80.7	Forest-Mixed Conifer (69.0 %) Forest-Conifer (9.0 %) Shrubland/Chaparral (8.9 %) Other (13.2 %)

Park Fire	California	40.082734 -121.749638	24/07/24	8:10 AM – 2:45 PM	65.0	53.2	Forest-Mixed Conifer (20. 6 %) Forest-Mixed Oak (8.1 %) Forest-Conifer (6.3 %) Shrubland/Chaparral (22.8 %) Grassland/Herbaceous (36.7 %)
Dimond Complex Fire	Oregon	43.268384 -122.301316	02/08/24	8:25 AM – 16:10 PM	18.1	116.0	Forest-Conifer (88.8 %) Other (11.2 %)
Red Fire	Oregon	43.491588 -122.034013	03/08/24	8:10 AM – 1:40 PM	28.3	89.2	Forest-Conifer (92.7 %) Other (7.3 %)
Middle Fork Complex Fire	Idaho	44.386634 -115.743022	26/08/24	7:25 AM – 12:25 PM	37.5	100.0	Forest-Conifer (53.2 %) Forest-Mixed Conifer (24.8 %) Shrubland/Chaparral (10.7 %) Grassland/Herbaceous (7.9 %) Other (3.5 %)
Wapiti Fire	Idaho	44.25896 -115.160892	27/08/24	7:05 AM – 12:30 PM	2.5	156.4	Forest-Conifer (53.2 %) Shrubland/Chaparral (19.8 %) Grassland/Herbaceous (8.1 %) Barren/Rock (12.4 %) Other (6.5 %)

035